ADVANCED MATERIALS
www.advmat.de

Thermoplasmonics in Solar Energy Conversion: Materials, Nanostructured Designs, and Applications

Bei Yang, Chenyu Li, Zhifeng Wang, and Qing Dai**

The indispensable requirement for sustainable development of human society has forced almost all countries to seek highly efficient and cost-effective ways to harvest and convert solar energy. Though continuous progress has advanced, it remains a daunting challenge to achieve full-spectrum solar absorption and maximize the conversion efficiency of sunlight. Recently, thermoplasmonics has emerged as a promising solution, which involves several beneficial effects including enhanced light absorption and scattering, generation and relaxation of hot carriers, as well as localized/collective heating, offering tremendous opportunities for optimized energy conversion. Besides, all these functionalities can be tailored via elaborated designs of materials and nanostructures. Here, first the fundamental physics governing thermoplasmonics is presented and then the strategies for both material selection and nanostructured designs toward more efficient energy conversion are summarized. Based on this, recent progress in thermoplasmonic applications including solar evaporation, photothermal chemistry, and thermophotovoltaic is reviewed. Finally, the corresponding challenges and prospects are discussed.

1. Introduction

In the global fight against climate change, China has pledged to achieve peak of carbon dioxide (CO_2) emissions before 2030 and reach carbon neutrality by 2060.[1,2] It is thus undoubtedly expected that this self-enforced commitment can accelerate the national energy transformation toward decarbonization, which exerts higher demands on the development of alternative renewable energy sources and related technologies.[3,4] Solar energy, as one of the most inexhaustible and green sources, has attracted significantly growing interest as it can be easily harvested and converted into heat, electricity, and chemical energy via photothermal, photovoltaic, and photochemical processes, respectively.[5,6] However, solar photonic energy is so dispersed from the ultraviolet (UV) to deep infrared (IR) regimes that nearly no single material or structure can harvest all its portions. Thus, how to maximize the harvesting and conversion of solar energy into other useful forms by rationally selecting materials and designing nanostructures as well as teaming them remains a daunting challenge.

In general, the utilization of solar energy involves various radiation-induced energy conversion processes, in which the light–matter interaction is strongly impacted by the photonic density of states (DOSs) in various materials. Notably, the DOS is termed as the number of “channels” for storing and/or routing the electromagnetic (EM) energy in a given medium.[7] Nanostructured materials with large DOS enable enhanced light trapping and thus they are preferred for solar technologies to improve the overall energy conversion efficiency. As one of the most promising candidates, plasmonic nanomaterials feature high DOSs due to their capability to focus light in the nanoscale.[8] For example, a noble-metal nanoparticle (NP) under specific illumination supports collective electronic resonance known as localized surface plasmon (LSP) resonance, enabling both enhanced light absorption and scattering. Then, the NP undergoes a significant increase in temperature due to the intrinsic loss in material that converts the absorbed photonic energy into heat. Nonetheless, this phenomenon has long been considered as a side effect that should essentially be minimized in traditional plasmonic applications. Only in the recent two decades, this field termed as thermoplasmonics has sprung up that uses plasmonic nanostructures as nanosources of heat and can be remotely controlled by light,[9,10] opening up new avenues for innovative practical applications. For instance, the rapid heating and ignition of metal NPs have been achieved by using this light-induced thermoplasmonic

---

B. Yang, Q. Dai
CAS Key Laboratory of Nanophotonic Materials and Devices
CAS Key Laboratory of Standardization and Measurement for Nanotechnology
CAS Center for Excellence in Nanoscience
National Center for Nanoscience and Technology
Beijing 100190, China
E-mail: daiq@nanoctr.cn
B. Yang, Q. Dai
Center of Materials Science and Optoelectronics Engineering
University of Chinese Academy of Sciences
Beijing 100049, China
C. Li
National Laboratory for Molecular Sciences CAS Research/Education Center for Excellence in Molecular Sciences Institute of Chemistry
Chinese Academy of Sciences
Beijing 100190, China
Z. Wang
Key Laboratory of Solar Thermal Energy and Photovoltaic System
Institute of Electrical Engineering
Chinese Academy of Sciences
Beijing 100190, China
E-mail: zhifeng@vip.sina.com

The ORCID identification number(s) for the author(s) of this article can be found under https://doi.org/10.1002/adma.202107351.

DOI: 10.1002/adma.202107351

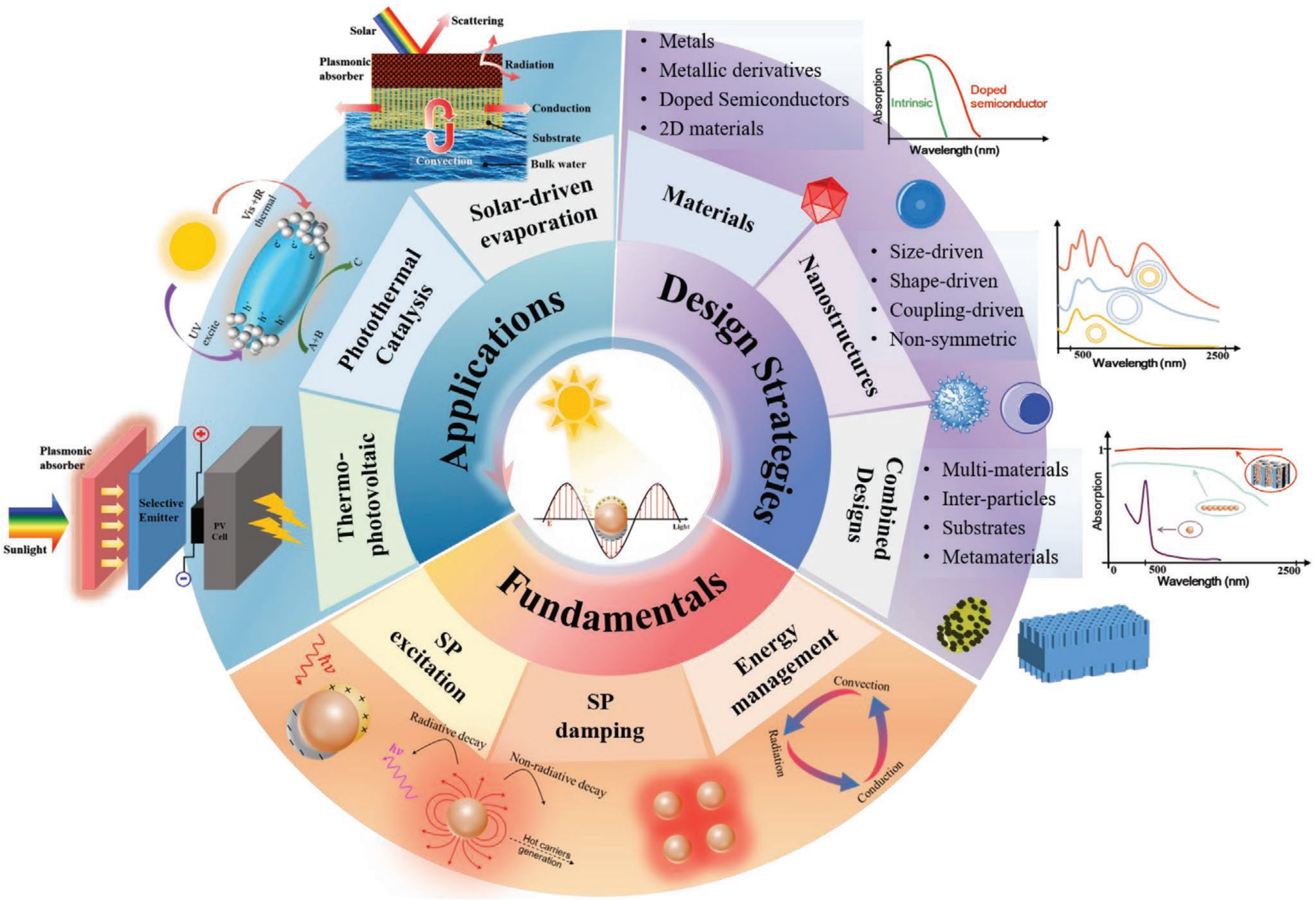

Figure 1. The schematic representing the guideline of this review on thermoplasmonics in solar energy utilization.

effect.[11] Other areas include cancer hyperthermia therapy,[12,13] cell biology,[14] heat-assisted magnetic recording,[15] nanofabrication,[16,17] nanochemistry,[18] solar energy harvesting,[19,20] and many others.[21,22] In particular, when incorporated into solar technologies, plasmonics enables ultrabroadband strong absorption because it offers tremendous opportunities for size-, shape-, and coupling-driven spectral shaping and tuning of material absorption behavior;[23] moreover, the resultant heating effects open new paths for solar thermal utilization. Therefore, thermoplasmonics presents itself as a promising solution to enhancing the harvesting and conversion efficiency of solar energy and has been increasingly investigated in various applications such as evaporation, photothermal catalysis, and thermophotovoltaics (TPV).

This review focuses on recent developments of thermoplasmonics in the solar energy field. The fundamental physics governing the principle of thermoplasmonics is elaborated, and basic strategies of material and nanostructured designs are summarized to tune the spectral absorption and to enhance the photothermal conversion efficiency. Then, recent advances are reviewed for targeted applications including solar evaporation, photothermal chemistry, and TPV. Finally, prospects and challenges are also discussed in detail. The outline of this review is illustrated in **Figure 1**. This review offers a comprehensive understanding of thermoplasmonics, especially the role it plays in solar technologies, and provides some useful clues for material and nanostructured designs toward highly efficient energy conversion in the renewable world.

2. Fundamental Physics

2.1. The Excitation of Surface Plasmons

The underlying physical mechanisms behind thermoplasmonics stem from both the excitation and damping of surface plasmons (SPs), which correspond to charge-density oscillations at the surface of a conductive material driven by the incident photons.[24] Further, SPs feature as EM surface waves that can be generally classified into the following two categories: the propagating SPs known as surface plasmon polaritons (SPPs) and the localized SPs denoted as LSPs. SPPs propagate as longitudinal waves along the metal–dielectric interfaces or thin metal films (**Figure 2**A). However, LSPs are localized standing waves in the vicinity of nanostructures with 3D spatial limitations such as NPs (Figure 2B).[25] Once getting excited upon illumination, both types of SPs confine the incident light into volumes much smaller than the diffraction limit, thus inducing significantly enhanced intensity of local electric fields around the nanostructure.[10,26] In this way, the light energy gets concentrated around the plasmonic nanostructures.

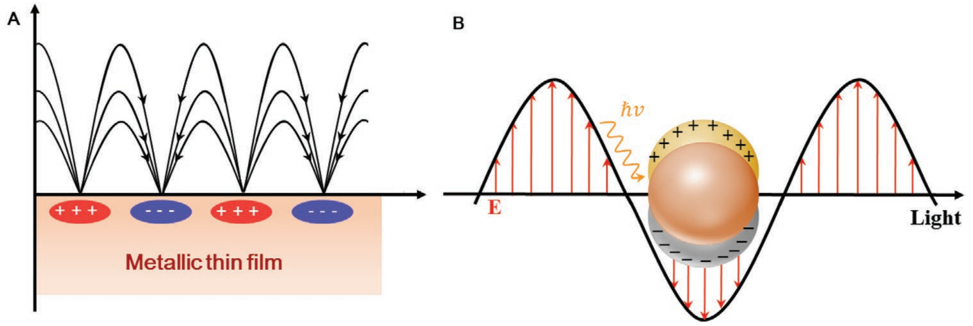

Figure 2. Schematic illustration of the two types of SPs: A) SPPs excited on a metal–dielectric interface along with the charge and electric field distributions and B) LSPs excited on a plasmonic metal NP.

2.2. The Damping of Surface Plasmons

Following the photoexcitation, LSPs on a metal NP undergo dephasing and decay at an ultrafast speed, through either radiatively reemitting photons or nonradiatively generating energetic charge carriers via Landau damping (**Figure 3**).[27] Notably, Landau damping is a pure quantum mechanical process during which a plasmon quantum is transferred into a single electron–hole pair excitation on a timescale ranging from 1 to 100 fs.[27,28] Owing to the strong energy confinement, these charge carriers from nonradiative LSPs decay have energies significantly higher than those from direct photo- or thermo-excitations, thus they are termed as "energetic" or "hot" carriers.[29,30] Three main steps are successively involved in the relaxation of these hot carriers on well-separated timescales:[10] 1) electron equilibration via electron–electron scattering within a few hundred femtoseconds; 2) lattice thermalization that leads to the increase in the local temperature of NP via electron–lattice scattering, occurring in a few picoseconds; and 3) lattice cooling through a much slower external heat diffusion to the environment via phonon–phonon scattering. The timescale of this final step ranges from 100 ps to 10 ns depending on the NP size as well as the thermophysical properties of both the material and the environment.[27] Noteworthy, collective heating effect may also occur if LSPs are strongly coupled in similar NPs existing adjacently (Figure 3), resulting in a uniformly distributed temperature field.[31]

In summary, thermoplasmonics involves several beneficial effects originating from the excitation and damping of SPs in nanostructures, including the enhanced light absorption and scattering, generation and relaxation of hot carriers, as well as localized/collective heating. These effects differ in temporal, spatial, and energy distributions, which can be flexibly tailored through delicate and careful selection of materials and nanostructured designs for specific purposes in a variety of applications.

2.3. Basic Mathematical Descriptions

To elucidate these processes, some basic mathematical descriptions of thermoplasmonics are presented in this section, in terms of three aspects including optical response, heat generation, and heat transfer.

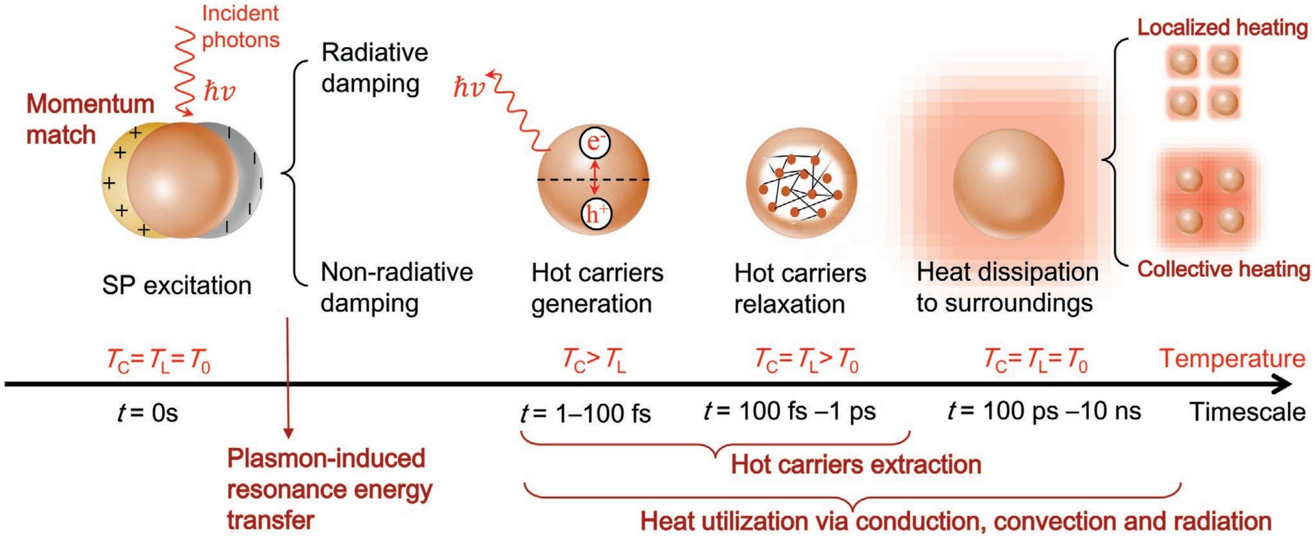

Figure 3. Fundamental physical processes involved in the damping of LSP at different timescales, following its excitation on a metal NP by laser pulse. In this figure, T_C, T_L, and T_0 denote the temperature of free carriers, lattice, and ambient environment, respectively. Redrawn from literature studies.[26,27]

2.3.1. Optical Response

Considering a spherical NP with a diameter d much smaller than the wavelength λ of incident light, i.e., $d \ll \lambda$, the surface electrons can be uniformly polarized by the incident field, which turns the NP into an EM dipole. In this case, the LSP response of this NP can be considered in quasistatic approximation and expressed in terms of the polarizability α[32]

$$\alpha(\omega) = \frac{\pi d^3}{2} \frac{\varepsilon(\omega) - \varepsilon_0}{\varepsilon(\omega) + 2\varepsilon_0} \tag{1}$$

where ε_0 and $\varepsilon(\omega)$ denote the permittivity of the surrounding medium and the NP, respectively. The latter is frequency-dependent and can be expressed as a complex quantity with a real part ε_1 signifying the polarization strength induced by the external electric field and an imaginary part ε_2 denoting the energy loss encountered in polarizing the material.[33] For most plasmonic materials, $\varepsilon(\omega)$ can be semiclassically approximated by using the Drude–Lorentz model[34]

$$\varepsilon(\omega) = \varepsilon_1 + \mathrm{i}\varepsilon_2 = \varepsilon_\infty - \frac{\omega_\mathrm{p}^2}{\omega^2 + \gamma^2} + \frac{\mathrm{i}\omega_\mathrm{p}^2\gamma}{\omega(\omega^2 + \gamma^2)} \tag{2}$$

$$\omega_\mathrm{p}^2 = \frac{n_\mathrm{e} e^2}{m^* \varepsilon_\infty} \tag{3}$$

where ε_∞ represents the high-frequency dielectric constant, γ indicates the damping constant denoting the scattering of free carriers, and ω_p represents the plasma frequency characterizing the speed at which electrons with free carrier concentrations n_e, elementary charge e, and effective mass m^* collectively response to the applied external electric field.

Equation (1) indicates that resonance occurs at the frequency ω when $\varepsilon(\omega) = -2\varepsilon_0$. This leads to both enhanced absorption and scattering, which correspond to sharp peaks in related spectra. The efficiency of these two processes can be, respectively, described by the absorption and scattering cross-section as follows[35]

$$C_\mathrm{abs} = k\mathrm{Im}(\alpha) - \frac{k^4}{6\pi}|\alpha|^2 \tag{4}$$

$$C_\mathrm{sca} = \frac{k^4}{6\pi}|\alpha|^2 \tag{5}$$

where $k = 2\pi/\lambda$ is the wavenumber. Their sum leads to the total light attenuation characterized by the extinction cross-section $C_\mathrm{ext} = C_\mathrm{abs} + C_\mathrm{sca} = k\mathrm{Im}(\alpha)$.

Notably, Equations (1), (4), and (5) are valid only for spherical NPs with relatively small sizes. For larger NPs, the dipolar approximation is no longer applicable because the size-dependent retardation effects become notable, where more rigid models as Mie's scattering model[35] are required. In case of more sophisticated geometries far away from spheres, numerical models such as finite element method (FEM),[36] finite-difference time-domain (FDTD),[37] etc., are required to solve the full EM field.

2.3.2. Heat Generation

The photonic energy absorbed by the NP can be simply calculated by using the absorption cross-section C_abs as follows

$$Q_\mathrm{abs} = C_\mathrm{abs} I \tag{6}$$

where I is the incident light intensity. In the case of a plane wave, $I = c\varepsilon_0|E_\mathrm{inc}|^2/2$, where $|E_\mathrm{inc}|$ denotes the incident electric field amplitude. This absorbed energy inevitably dissipates into heat due to the Joule heating effect, thus it can also be calculated by integrating the heat power density $q(\boldsymbol{r})$ inside the NP over its volume V, i.e., $Q_\mathrm{abs} = \iiint q(\boldsymbol{r})\,\mathrm{d}V$, where $q(\boldsymbol{r})$ reads

$$q(\boldsymbol{r}) = \frac{1}{2}\mathrm{Re}\left[\boldsymbol{J}^*(\boldsymbol{r})\cdot\boldsymbol{E}(\boldsymbol{r})\right] \tag{7}$$

where $\boldsymbol{J}(\boldsymbol{r})$ is the complex amplitude of the electronic current density in the NP. As $\boldsymbol{J}(\mathbf{r}) = \mathrm{i}\omega\boldsymbol{P}$ and $\boldsymbol{P} = \varepsilon_0\varepsilon(\omega)\boldsymbol{E}$, the $q(\boldsymbol{r})$ ends up with

$$q(\boldsymbol{r}) = \frac{\omega}{2}\varepsilon_2\varepsilon_0\left|\boldsymbol{E}(\boldsymbol{r})\right|^2 \tag{8}$$

Evidently, $q(\boldsymbol{r})$ directly scales with $|\boldsymbol{E}(\boldsymbol{r})|^2$ as well as ε_2. Moreover, these two factors are contradictory because a larger ε_2 often corresponds to a greater loss, which results in a less enhanced electric field, i.e., a smaller $|\boldsymbol{E}(\boldsymbol{r})|$. This is an important aspect to consider when selecting appropriate materials to design efficient plasmonic nanoheaters.

2.3.3. Heat Transfer

The LSP-mediated heat generation inside the NP inevitably results in the increase in temperatures of both the NP and its surroundings. Based on the general heat transfer equation, the transient temperature fields inside and outside the NP can be, respectively, expressed as[10,32]

$$\rho C_\mathrm{p}\frac{\partial T(\mathbf{r})}{\partial t} = \nabla\cdot\left[\kappa(\mathbf{r})\nabla T(\mathbf{r})\right] + q(\mathbf{r}), -r \le |\mathbf{r}| \le r \tag{9}$$

$$\rho C_\mathrm{p}\frac{\partial T(\mathbf{r})}{\partial t} = \nabla\cdot\left[\kappa_\mathrm{s}(\mathbf{r})\nabla T(\mathbf{r})\right], |\mathbf{r}| > r \tag{10}$$

where κ and κ_s, respectively, denote the thermal conductivity of the plasmonic NPs and the surrounding media. Moreover, for a spherical NP with radius r, its temperature reaches a steady state after tens of nanoseconds. By relating Equations (6) and (9), the steady temperature rise inside the NP can be calculated by

$$\Delta T_\mathrm{NP} = \frac{Q_\mathrm{abs}}{4\pi\kappa_\mathrm{s} r} = \frac{C_\mathrm{abs} I}{4\pi\kappa_\mathrm{s} r} \tag{11}$$

For the case where several adjacent NPs are illuminated simultaneously, the temperature rise of NP j is also caused by the contribution of neighboring NP i heating their surroundings, which can be given as[31,38]

$$\Delta T_{\mathrm{NP},j} = \frac{C_{\mathrm{abs},j} I}{4\pi\kappa_\mathrm{s} r_j} + \sum_{i \ne j}\frac{C_{\mathrm{abs},i} I}{4\pi\kappa_\mathrm{s}\left|r_i - r_j\right|} \tag{12}$$

Noteworthy, the last term in Equation (12) may become dominant even for a sparse distribution of NP, which gives rise to the so-called collective photothermal effects. Compared to localized heating around single NP leading to isolated hotspots, the collective heating effect features a strong overall temperature rise and a uniform temperature distribution.[21] This collective effect can be flexibly manipulated via controlling the NP size, the interparticle distance, the irradiation intensity, as well as the characteristic diameter of the illumination.

2.3.4. More Factors to Be Considered

Ultrashort Pulse Illumination: The photothermal responses of plasmonic materials highly depend on the irradiation regime, e.g., continuous-wave (CW) illumination and pulsed (nanosecond, picosecond, and femtosecond) lasers. The key lies in the comparative analysis carried out between timescales of the illumination duration τ and the electron–phonon energy relaxation time $\tau_{\text{e-ph}}$ (10^{-10}–10^{-12} s). In cases of CW such as sunlight or nanosecond-pulsed lasers ($\tau \gg \tau_{\text{e-ph}}$), the hot electrons have enough time to transfer their energy to the phonons, which aids in achieving an equilibrium state between them during illumination. The entire process is quasiequilibrium and thus the classical heat diffusion equation presented in Section 2.3.3 is valid. However, for the sub-picosecond and femtosecond-pulsed lasers ($\tau \ll \tau_{\text{e-ph}}$), the electronic light absorption is completed before the electron–phonon scattering occurs. In other words, the electrons heat up, while the lattice temperature remains unchanged within this ultrashort pulse duration.[39] The electronic heat capacity is significantly less (1–2 orders of magnitude) than that of the phonons; therefore, it produces transient electron temperatures far beyond the lattice. The electronic temperature T_e resulting from the internal thermalization of hot electron gas varies from 100 to 1000 K depending on the pump fluence and pulse duration. However, the lattice temperature T_l increases more slowly to much lower values. This ultrafast dynamics in thermoplasmonics has been widely studied by time-resolved pump–probe spectroscopy and by using appropriate modeling.[40] In this context, the classical description presented in Section 2.3.3 is no longer valid and often the two-temperature model that distinguishes the transient temperatures of electrons and phonons is required due to their highly nonequilibrium distribution. Besides, this ultrashort pulse may trigger a strong optical nonlinearity in plasmonic NPs due to the nonthermal electronic distribution and multiphoton excitation, which in turn modifies the absorption property.[41] A complete description of this ultrafast optical nonlinearity in plasmonic systems has been recently developed, based on which a novel approach for ultrafast polarization control was proposed by taking advantage of the inhomogeneous spatiotemporal distribution of photogenerated hot carriers with a picosecond laser pulse.[42]

Nonlinear Thermo-Optical Effects: A direct result of thermoplasmonics is the temperature rise of the NP, which in turn affects its optical response including the absorption and scattering efficiencies. Further, this nonlinear thermo-optical effect becomes prominent when high temperature or high-intensity illumination is involved. The main channel through which the temperature impacts the optical response is the damping factor γ in $\varepsilon_2(\omega)$ (Equation (2)).[43] Both the electron–electron and electron–phonon scattering rates increase with increasing temperatures, thus translating into larger damping losses. Recent experimental measurements revealed that the relative increase of $\varepsilon_2(\omega)$ for Ag at 600 K to its room-temperature value was about 500% at around its resonant wavelength.[44] This change finally resulted in the bleaching (intensity reduction) of the LSP band together with the broadening of the spectral envelope.[17] In this context, numerical modeling is often required where both the Maxwell and heat equations need to be self-consistently solved with a temperature-dependent permittivity, relying on either experimentally measured data[45] or classical approximation such as the Drude–Lorentz model.[43] For instance, this nonlinear thermo-optical effect has been particularly treated and engineered to control the heat dissipation in plasmonic nanorods (NRs).[46]

3. Material Selection and Nanostructured Designs

The first step to achieve high-performance devices for solar-driven applications is to design solar absorbers enabling both ultrabroadband light absorption and efficient energy conversion. Nonetheless, the SP-enhanced light absorption exhibits narrow peaks at related resonant wavelengths, leading to rather limited absorbed energy due to the dispersed distribution of solar spectral energy (**Figure 4**A). This issue can be addressed by elaborating plasmonic material selection and nanostructured designs, attributed to the high tunability of SPs. Thus, this review mainly focuses on some basic strategies in terms of selecting appropriate plasmonic materials, tuning SP responses via single NP designs (size and shape), as well as exploiting coupling effects in NP assemblies with well-designed substrates (Figure 4B–D).

3.1. Material Selection and Tunability

The optical response of a conductive material to the incident light depends on its complex polarizability or dielectric permittivity.[24,35] The latter describes the material's bulk properties, including contributions from transition between electronic bands, excitation of vibrational modes, and movement of free carriers.[35,47] The effect of n_e on $\varepsilon(\omega)$ is quantitatively reflected by Equations (2) and (3). Decrease in the value of n_e results in smaller ω_p, i.e., redshifts of the SP peaks to longer wavelengths (**Figure 5**). Carrier mobility and interband losses are the two other important factors that affect the optical properties of plasmonic materials. Lower carrier mobilities translate into higher material losses due to scattering effects of defects in solids;[48] however, interband losses occur when electrons jump to higher energy levels by absorbing incident photons, which corresponds to the dominant loss mechanism in materials at optical frequencies.[33] These two loss mechanisms together with losses from intraband transitions constitute the inherent material loss that can be well reflected by ε_2.[49] Furthermore, Equations (2) and (3) clearly illustrate that higher values of n_e correspond to larger values of ε_2, i.e., higher energy losses.

Figure 5A presents the basic optical properties for various plasmonic materials based on the following three important

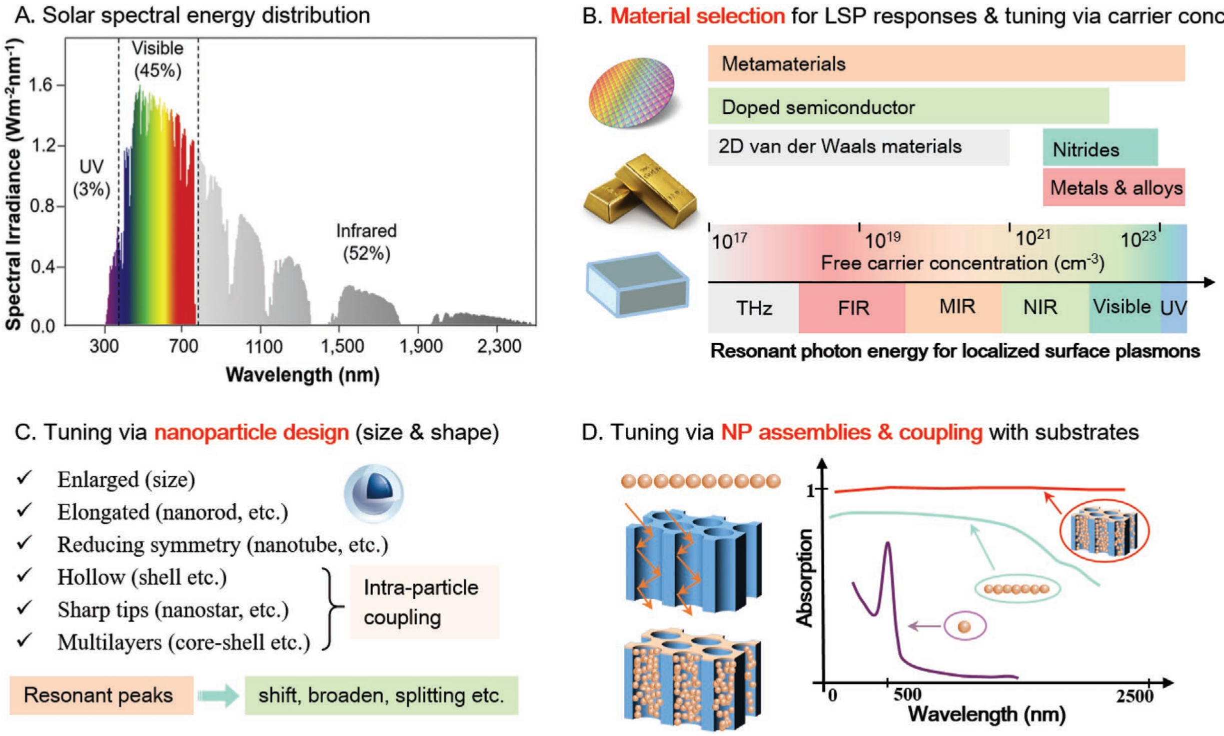

Figure 4. Basic strategies for material selection and nanostructured designs: A) solar spectral energy distribution; B) material selection for characteristic LSPs and tuning via n_e; C) tuning LSPs via single NP designs by varying sizes and shapes; and D) tuning LSPs by exploiting coupling effects in NP assemblies and substrate engineering.

parameters: carrier concentration, carrier mobility, and interband losses.[48] In order to excite SPs, the n_e has to be high enough to provide a negative real part of dielectric permittivity ($\varepsilon_2 < 0$). Moreover, ε_2 should also be small enough to ensure well pronounced SPs ($\varepsilon_1 \gg \varepsilon_2$).[23] Although it seems that higher inherent material losses contribute to heat generation (Equation (8)), it has been well demonstrated that the SP-induced heating capacity generally depends on $1/\varepsilon_2$.[50] Therefore, ideal thermoplasmonic materials for solar technology should have sufficiently high n_e and mobility as well as relatively low losses, i.e., lying in the left end of the plot with resonant wavelengths ranging from UV to near-infrared (NIR) region (Figure 5A).[48] Unfortunately, nearly no such material exists. Herein, the merits and drawbacks of various plasmonic materials, including metals, metallic derivatives, heavily doped semiconductors, and 2D materials, together with the selection and tuning strategies for their utilization in solar-driven applications are summarized.

3.1.1. Metals

Noble metals such as gold (Au) and silver (Ag) are the two most commonly used metal materials in thermoplasmonics, due to their high n_e and relatively small Ohmic losses featuring pronounced SP responses within ranges from the visible to NIR region (Figure 5A).[51–53] However, they suffer from strong interband transitions that induce additional losses at optical frequencies, thus limiting the tunable flexibility for robust SPs.[34] Besides, Ag tends to get oxidized or sulfurized rapidly under atmospheric conditions, which strongly degrades its plasmonic properties. Moreover, they are rare metals and thus expensive that hinders their large-scale industrial applications.

Copper (Cu) and aluminum (Al) are envisioned as promising alternatives to Au and Ag as they are earth-abundant and significantly more cost-effective. Cu shows similar SP responses to Au (**Figures** 5A and **6**) but suffers from chemical instability under atmospheric conditions.[54] By contrast, Al exhibits strong SPs in the UV range, and demonstrates the strongest near-field enhancement and the highest photothermal efficiency.[9,50] Attributed to its high ω_p, Al supports high-quality SPs throughout the UV–vis–IR regions.[55] Although Al also suffers from rapid oxidation, it tends to form a 3 nm thick layer of Al_2O_3 that acts as an effective passivation layer to prevent it from further denaturation. Notably, it has been demonstrated that this passive layer does not strongly affect the SP response of Al.[50] Owing to these merits, Al-based plasmonics has been increasingly studied for a wide variety of practical applications.[56–61] Nonetheless, one inherent limitation for Al crystals is the relatively broad linewidths of their SPs at visible frequencies due to their large radiative losses resulting from interband transitions.[62,63]

Refractory metals including tungsten (W), tantalum (Ta), and molybdenum (Mo) have drawn substantial interest due to their high melting points (Figure 5C). Their capability to remain chemically stable at temperatures above 2000 °C makes them very attractive for high-temperature applications. However, these refractory metals exhibit SP resonances mostly in the NIR region with relatively high losses.[64]

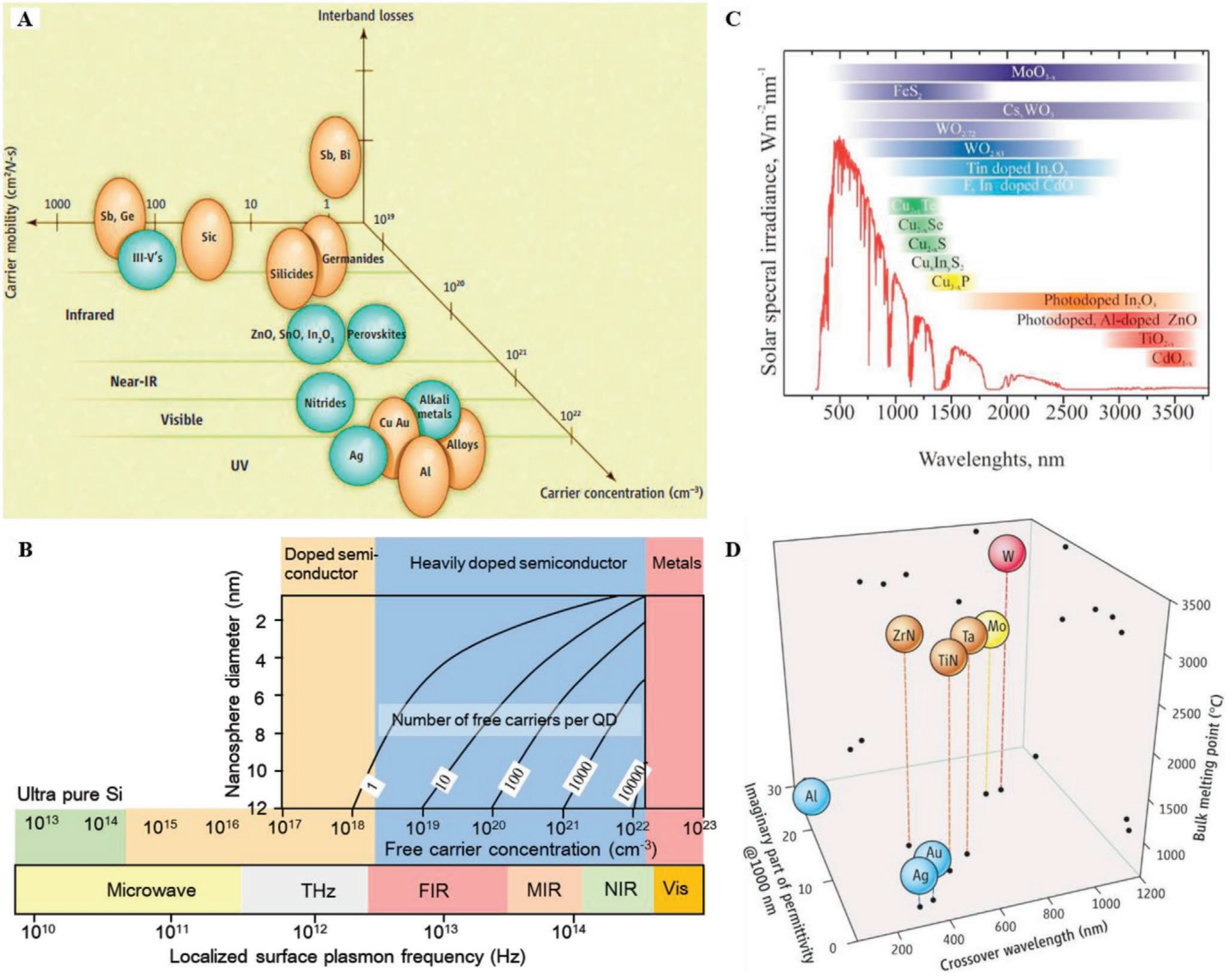

Figure 5. Material selection for thermoplasmonics in solar energy utilization. A) Optical properties of various materials based on carrier concentration, carrier mobility, and interband losses. Reproduced with permission.[48] Copyright 2011, AAAS. B) Doped semiconductors as candidates and related LSP frequencies depending on n_e and doping constraints, redrawn from the reference.[66] C) The solar spectrum and related semiconductor NCs with tunable LSP-mediated absorption ranges. Reproduced with permission.[19] Copyright 2021, Elsevier. D) Refractory plasmonic materials. Reproduced with permission.[64] Copyright 2014, AAAS.

UV metals, a family of metals that support SPs in the UV range, including cobalt, chromium, nickel, palladium (Pd), platinum (Pt), titanium, and others have also been explored.[50] However, they are not really of practical interest in thermoplasmonics except for Pd and Pt whose catalytic properties are favorable for related nanochemistry applications. Moreover, alkali metals have attractive plasmonic properties; nonetheless they are out of consideration due to their extremely high chemical reactivity.[34]

Except for high losses and poor chemical stability for most metals, other challenges when using metals in thermoplasmonics are also encountered as well, including nanofabrication and surface roughness, both of which might induce additional losses.[65] Besides, the major drawback of metals is that their optical properties cannot be easily tuned via applied external electric, optical, or thermal fields, owing to their high n_e.[34]

3.1.2. Metallic Derivatives

The losses associated with the abovementioned pure metals partly arise from their high n_e. Thus, an overall approach to address this issue is to mix them with less conductive metals or nonmetals, giving rise to alloys, intermetallics, or metallic compounds (silicides, germanides, borides, carbides, nitrides, oxides, etc.).[48] This can be achieved by alloying/reacting two or more elements, thus related SP responses can be finely tuned by adjusting the proportion of each alloyed material/reactant.[65] For example, Au–Ag alloy NPs exhibit LSPs over a broad range of UV–vis spectra and present a distinct redshift with increasing Au fraction.[67] A general rule is that the optical properties become worse than the best of the metals being alloyed, and intermetallics with more atoms in a unit cell usually suffer from higher optical losses.[65]

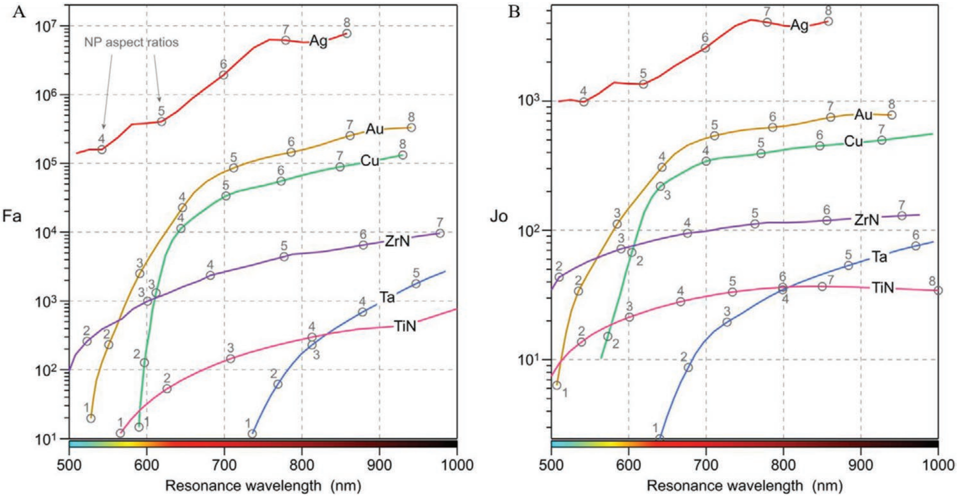

Figure 6. Thermoplasmonic properties for various materials: A) calculated Faraday number denoting the quantitative estimation of near-field enhancement, and B) Joule number quantifying the ability of a plasmonic material to generate heat, plotted as a function of the resonance wavelength of ellipsoids made of various materials. Reproduced with permission.[50] Copyright 2015, ACS.

As representative examples of metallic compounds, transition metal nitrides, in particular, titanium nitride (TiN) and zirconium nitride (ZrN), have been considered as promising alternatives to noble metals due to both their excellent refractory and plasmonic properties.[68] They possess outstanding thermal stability under temperatures above 2900 °C (Figure 5C).[64] Unlike refractory metals, they support SPs in the visible and longer wavelength regions and exhibit a good impedance match with air.[68] However, they exhibit higher inherent losses than noble metals, owing to their larger carrier relaxation rates and interband transitions in optical ranges.[65] This renders them as poorer near-field enhancers than Au, but more efficient nanoheaters in some cases (Figure 6A,B). Notably, TiN has been increasingly explored for high-temperature plasmonic applications.[69–73]

3.1.3. Heavily Doped Semiconductor Crystals

Heavily doped semiconductor nanocrystals (NCs) have emerged as potential thermoplasmonic materials.[74,75] They possess distinct advantages over metals, e.g., the capability to tune SP responses via chemical doping, accessible SP frequencies spanning from visible to far-infrared (FIR) ranges, flexibility to post-synthetically tune the SP characteristics, etc.[25,76–78]

In doped semiconductors, the free carriers can be either electrons (n-type dopant) or holes (p-type dopant) depending on the oxidation state of the dopant relative to host ions. Heavy doping to high-enough concentration is necessary for both types of semiconductors to induce SPs within solar spectral ranges (Figure 5B,D). Metal chalcogenides, including $Cu_{2-x}S$, $Cu_{2-x}Se$, $Cu_{2-x}Te$, $Fe_{1-x}S_2$, etc., are p-type doped semiconductors with a metal (cation) vacancy. By contrast, most metal oxides, e.g., In_2O_3, CdO, ZnO, MoO_{3-x}, WO_{3-x}, etc., are n-type materials doped with some equilibrium oxygen (anion) vacancy.[25,79,80] For instance, Cu chalcogenide binary semiconductor NCs feature SPs mainly within wavelengths of 800–2000 nm due to their relatively low n_e of 10^{21} cm^{-3}. However, further increase in n_e was demonstrated in $Fe_{1.0}Cu_{1.0}S_{1.8}$, extending SP responses to the visible range.[79] Furthermore, $WO_{2.83}$ NC and MoO_{3-x} nanosheets with tunable vacancies have also been constructed to enhance the light absorption mediated by SPs from visible to NIR ranges.[81] However, the doping level for many semiconductors is limited due to concerns about the solid solubility limit, the fraction of active dopants, and the doping compensation effects.[33,82] Challenges such as difficulties in controlling SPs of metal oxides via dopant-dependent phase transformation and ligand exchange, instability of metal chalcogenides under high temperature, or laser illumination also remain.[83]

3.1.4. 2D Materials

Atomically thin 2D materials are promising plasmonic materials with distinct advantages over their bulk counterparts from both scientific and technological perspectives.[84,85]

The 2D van der Waals (vdW) materials, including graphene,[86] transition-metal dichalcogenides,[87] black phosphorus,[88] and many other materials are among the most investigated types.[89,90] The high tunability, large doping concentration range, and existence of favorable depolarization factors allow better control over their SP responses.[85] Electrostatic gating or chemical doping techniques have been widely adopted to increase their n_e. For instance, 2D MoS_2 supports SPs in the FIR and terahertz regimes due to a low n_e in the range of 10^{12}–10^{14} cm^{-3}. Through Li^+ intercalation, ultradoped 2D MoS_2 nanoflakes were synthesized, which shifted the SP resonance to the visible and near-UV ranges.[91] However, tuning SPs over such a broad range of wavelengths is very difficult for most 2D vdW materials. Even for graphene, known as a semimetal, its SPs can be electrically, chemically, or optically tuned mostly within ranges of THz–mid infrared (MIR), and into the NIR in some cases.[90] This leads to its rather limited usage in plasmonic solar-driven applications. Besides, the synthesis of large-area single-crystalline 2D vdW materials still remains a challenging task that also limits their practical applications.[23]

Another family of 2D layered materials showing significant research potential is MXene, i.e., 2D carbides and nitrides of

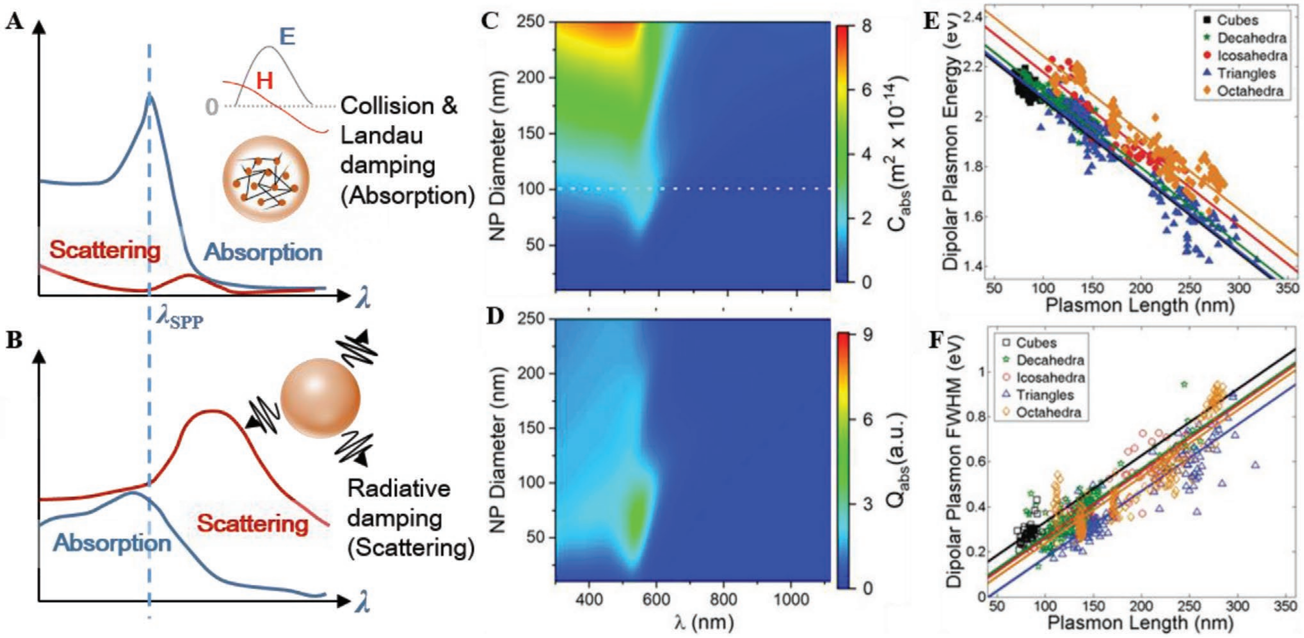

Figure 7. Size-driven tunability for LSP responses. A,B) Variation of inherent damping mechanisms with NP sizes: (A) absorption-induced nonradiative damping dominating smaller-sized NPs; (B) scattering-induced radiative damping dominating larger-sized NPs. Both are redrawn from the reference.[26] C,D) Absorption (C) cross-section and (D) efficiency of a single Au NP as a function of the NP radius and wavelength under illumination by a plane wave. Reproduced with permission.[32] Copyright 2019, ACS. E,F) Size-dependent dipolar plasmon (E) energy and (F) FWHM regardless of the NP shapes. Reproduced with permission.[101] Copyright 2012, ACS.

transition metals, which are produced by selective etching of strongly bonded layered solids.[92,93] Interestingly, they often have high metallic conductivity ($n_e = \approx 10^{22}$ cm^{-3}) and possess chemically tunable plasmonic properties.[94] Their optical properties depend on the type and structure of the M and X sites as well as on the stoichiometry of surface terminations, thus providing the scope for high tunability.[95] Different MXenes support SPs spanning across the entire vis–NIR spectral region.[93] They also show strong absorption in the UV range owing to interband transitions. All these merits render them attractive in solar–thermal applications.[96,97] For instance, Ti_3C_2, as the most typical representative of MXenes, has been well demonstrated to exhibit better solar absorption than carbon nanotubes (CNTs), yielding an internal photothermal conversion efficiency of ≈100%.[98] Benefited from SP-induced strong light absorption and heating effects, 2D MXenes act as promising 2D building blocks to efficiently harvest solar energy and utilize the translated thermal energy.[99]

3.2. Nanostructured Designs

Although the frequency of LSP is primarily controlled by the n_e of the material, it can also be flexibly tuned by varying the size and shape of the nanostructures and exploiting the coupling effects of NP assemblies with substrates.

3.2.1. Size Effects

Change in the size of plasmonic NPs is the most straightforward approach to tune their LSP responses. In general, an increase in the NP size leads to the redshift and broadening of the resonant peaks (**Figure 7**A–D). This stems from the retardation effects occurring in the EM interaction between distant charges that feature nonuniform oscillation states on larger NPs.[9] From the perspective of energy conversion, the total extinction energy increases with increasing NP sizes. However, the dominant role changes from the absorption for smaller NPs to the scattering for larger ones (Figure 7A,B), indicating the energy decay competing between the radiative and nonradiative mechanisms. The broadening of resonant peaks originates from the strongly enhanced radiative damping in larger NPs, resulting in a reduced amount of energy that can be stored in the LSP. This in turn reduces the accessible maximum local electric field intensity.[100] In this sense, smaller NPs are more efficient absorbers than larger ones and may be more favorable for thermoplasmonic applications.[32] Figure 7E,F further illustrates the distribution of both energy and full width at half maximum (FWHM) for dipolar plasmons as a function of plasmon length, which is defined as the distance along which the oscillation occurs. The plasmon energy stored in LSPs drops with the increase of this effective size parameter, regardless of the shape of NPs. Correspondingly, the LSP linewidth increases as a direct result of radiative damping.

3.2.2. Shape Effects

Apart from sizes, variation in the NP shape can also be exploited to tune its LSP responses, because the nanostructured shape provides the boundary conditions that strongly affect the light–matter interaction. This tunability roots in either the

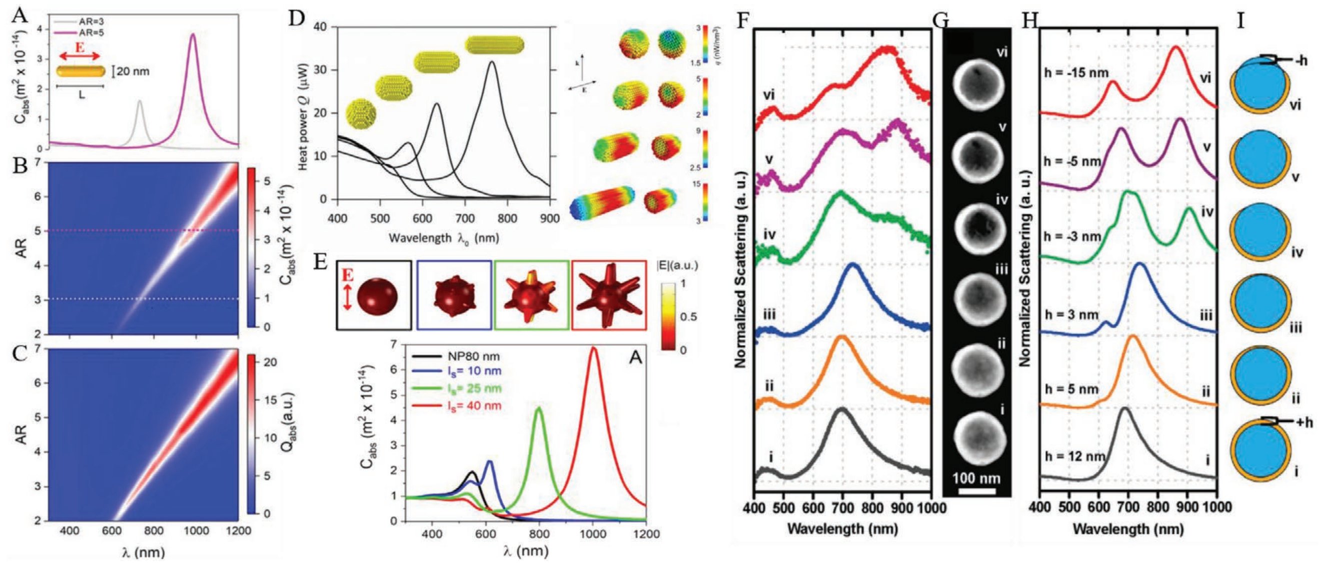

Figure 8. Shape-driven tunability for LSP responses. A–C) LSP responses of Au NRs with various ARs: (A) Comparison of C_{abs} for Au NRs with AR being 3 and 5; contour maps for absorption (B) cross-section and (C) efficiency as a function of AR and incident wavelength for the longitudinal mode. Reproduced with permission.[32] Copyright 2019, ACS. D) Calculated spectra of heating power and the corresponding contours of resonant heat power density for four same-sized Au NPs with various ARs. Reproduced with permission.[102] Copyright 2009, AIP. E) Absorption spectra of Au nanostars with increasing spike length l_s. Reproduced with permission.[32] Copyright 2019, ACS. F–I) Scattering spectra and geometry of a single nanoshell with various asymmetries: (F) experimental results from polarization-dependent dark-field microspectroscopy; (G) Environmental scanning electron microscopy (ESEM) images; (H) numerical results via FEM simulations; and (I) the corresponding simulated geometries. Reproduced with permission.[104] Copyright 2009, ACS.

deviation from dipole oscillation or the coupling between elementary plasmons in a single NP.

The most typical example is the NR obtained by elongating the spherical shape.[51] Two typical LSP modes, namely, transversal and longitudinal, exist in NRs corresponding to the electron oscillations polarized along the long axis and the radial direction, respectively. By increasing its aspect ratio (AR), i.e., the ratio of length to diameter, the LSP frequency of the longitudinal mode redshifts from the visible to NIR region (**Figure 8**A–C).[32] Besides, shape-directed manipulation of heating effects can also be achieved. Compared to spheres with equal volume, NRs are more efficient nanoheaters (Figure 8D), owing to their larger surface area-to-volume ratio, thus enabling more surface electrons to participate in resonance.[102] The NR with AR of 3 yields a maximal heat power density about a 4 times increase over that of the same-sized sphere (Figure 8D).[102] Based on this perspective, Au NRs are among the best plasmonic absorbers and the most efficient photothermal converters.

On the other hand, manipulation of the NP shape can lead to strong intraparticle coupling that distinctively alters the absorption property.[103] Core–shell structure and nanomatryoshka are typical examples. The former often consists of a dielectric core and a metallic shell or vice versa; however, the latter is referred to as a four-layer concentric NP consisting of alternating dielectric and metallic layers. The resultant LSP responses of these NPs can be understood as the coupling/hybridization of elementary plasmons supported by nanostructures with elementary geometries.[105] **Figure 9**A illustrates that the LSP responses of nanoshells can be attributed to the coupling phenomenon between the essentially fixed-frequency plasmon response of a spherical core and that of a nanocavity, both of which are highly geometry-dependent. For the four-layer nanomatryoshka made of silica (SiO_2) and Au, the thickness of the dielectric spacer layer determines the coupling strength between plasmons of the inner and outer nanoshell, which finally controls the energy distribution of the hybridized plasmons (Figure 9B,D). This physical image of plasmon hybridization guides general principles to design complex nanostructures with arbitrary shapes.

Other strategies that exploit this intraparticle coupling effect to shift, split, and broaden the LSP peaks include the generation of protrusions or indentations on NP surfaces (nanostars,[106] nanoflowers,[107] concaves,[108] cubes,[59] nanoantennas,[109] etc.), reduction in symmetry of the nanostructure (highly anisotropic shapes),[110] construction of hollow structure (hollow shells,[111] rings,[112] cups,[113] nanocages,[114] etc.), and others. For nanostars and similar geometries, intraparticle coupling effects are induced between these sharp tips as well as between the tip and the core modes. This makes their absorption very sensitive to their spike length, l_s. A distinct redshift of the absorption peak occurs from wavelengths of about 600–1000 nm when increasing the spike length from 10 to 40 nm (Figure 8E).[32] Moreover, these sharp protrusions often result in the generation of hotspots with the highest local electric field intensity, known as the "lightning rod effect,"[8,24,36] and have been demonstrated to lead to intense photothermal conversions.[109] Breaking and reducing symmetry as well as creating hollow structures can effectively broaden the LSP peaks. NPs with higher symmetry, such as spheres, cubes, and triangular plates, exhibit higher and sharper absorption peaks.[103] Similarly, for a given size of NP, the plasmon energy changes with the variation in shapes in the following order: triangles ≈ cubes < decahedra < icosahedra < octahedral, following the general

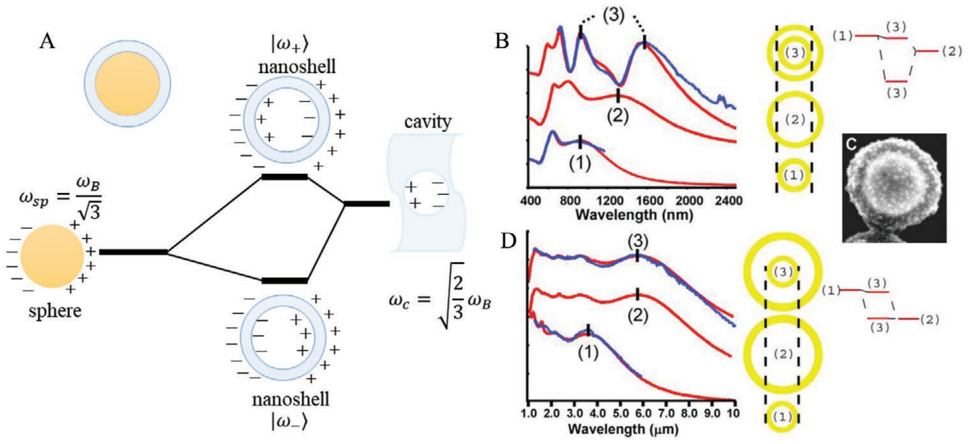

Figure 9. Exploration of intraparticle coupling to tune LSP responses of nanostructures: A) an energy-level diagram describing the plasmon hybridization in metal nanoshells resulting from plasmon coupling between the spherical core and the cavity, B,D) experimental (blue) and calculated (red) extinction spectra for elementary nanostructures of the nanomatryoshka for the cases of (B) strong coupling and (D) uncoupled plasmons, and C) scanning electron microscopy (SEM) images of the four-layer concentric nanoshell. Reproduced with permission.[105] Copyright 2019, AAAS.

trend expected for highly anisotropic to sphere-like NPs.[101] More direct observation for the effects of reduced symmetry for nanostructures on their LSP responses is shown in Figure 8F–I. By controlled reshaping of an individual Au nanoshell, the transformation of its plasmonic properties, in particular, the splitting of plasmon modes and the onset of electroinductive plasmons are displayed.[104]

Numerical studies on the heating effects indicate that small, flat, elongated, or sharp NPs appear to be much more efficient heaters than massive nanostructures.[102] This result is attributed to the fact that the incident photons can penetrate more easily into the thinner and smaller NPs to allow more plasmonic metals to get involved in heating.

3.2.3. Coupling Effects

Furthermore, LSP responses can also be flexibly tailored via manipulating coupling effects not only from adjacent NPs, but also from interactions with the supporting substrates or other surrounding media.

Interparticle coupling effects can be exploited to broaden and enhance light absorption via careful arrangement of the NP assemblies. Dimers, for example, i.e., two adjacent NPs separated by a nanogap, allow for the generation of strongly enhanced localized electric field in the gap and also remarkable photothermal effects, resulting from the effective coupling of SPs excited on each NP (**Figure 10**A).[115,116] Similar assemblies include hexamers,[117] heptamers,[118] nanoarrays,[14] nanochains,[119] vesicular/clustered gold vesicle (GV),[120] etc. Notably, the optical and thermal responses of this type of NP assemblies are highly sensitive to the number of NPs involved, the gap distance, and the direction of the incident light, together with the size and shape of each NP. This provides great flexibility to tune the LSPs coupling, thus achieving the most desired responses. For instance, Au NPs hierarchically assembled into vesicle architectures wrapped with a vesicular membrane allow the LSP peaks to extend to NIR region and yield a very high photothermal conversion efficiency due to ultrastrong plasmonic coupling between adjacent Au NPs (Figure 10B–D).[120] In this design, both the parameters of NP assemblies and the hollow interior play important roles in the enhanced absorption and photothermal conversion. Furthermore, it has also been demonstrated that plasmonic NPs organized into ordered arrays with spacing comparable to the light wavelength can produce even greater field enhancement and higher-quality resonance by exploiting short- and long-range interactions, compared to that of random NP clusters.[121,122]

A supporting substrate for plasmonic nanostructures may also distinctively alter their LSP responses by promoting the coupling and hybridization of plasmon modes,[123,126,127] and/or trapping photons via multiple scattering.[128,129] In general, for a NP deposited on a substrate, the substrate breaks and reduces the symmetry of the photon scattering and thus leads to the shifting, broadening, and splitting of the original LSP peaks of the NP.[123] For a plasmonic NP placed adjacent to substrates with various geometries, the coupling strength of SPs between them depends on the permittivity of the substrate. The metallic substrates often induce strong coupling effects; however, the dielectrics lead to weaker interactions where the LSP of the NP couples only to its image of surface charges. Moreover, the contact surface area between the NP and the substrate is also significantly important as it affects the hybridized state of plasmon modes, with larger hybridization induced by a larger contact area (Figure 10E–G). In case of a nanocube, a nearby dielectric mediates an interaction between bright dipolar and dark quadrupolar modes, resulting in the generation of bonding and antibonding hybridized modes.[123] On the other hand, well-designed substrates as porous or hierarchical structures can trap photons via promoting multiple scattering, thus further enhancing the light absorption.[128,129]

In case of the heating effects, both localized and uniform temperature distribution can be achieved by controlling the total number of NPs, their relative distances, and the illumination conditions. The substrates/surroundings also significantly affect the final temperature distribution of plasmonic NPs, as they control how fast the LSP-induced heat can transfer and how far it can penetrate externally.[125,130] A general trend is

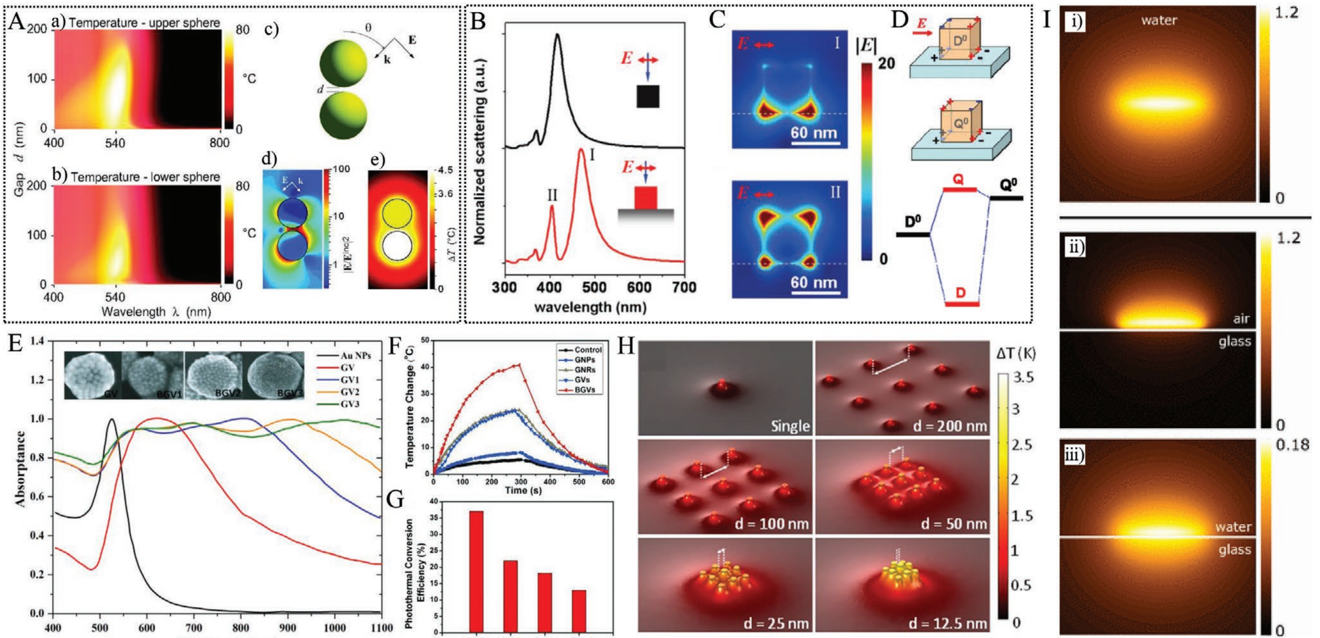

Figure 10. Coupling-driven tunability of LSPs and related heating effects. A) Coupling between Au dimer: a,b) temperature distribution as a function of light wavelength and gap distance; c) sketch of the dimer; d) electric near-field intensity; and e) the corresponding temperature field. Reproduced with permission.[115] Copyright 2010, ACS. B–D) Interparticle coupling effects of Au clusters: (B) measured absorptance spectra and SEM images of GV; (C) temperature rise; and (D) photothermal conversion efficiency. Reproduced with permission.[120] Copyright 2013, Wiley. E–G) Coupling of an Ag cube with substrates: (E) normalized scattering spectra of Ag cube in vacuum (black) and on a glass substrate (red); (F) the corresponding electric field amplitude at two scattering peaks in (E); (G) schematic illustration of the substrate-mediated energy level interaction. Reproduced with permission.[123] Copyright 2011, ACS. H) Calculated temperature profiles of Ag NP arrays arranged in a square lattice with various lateral distances. Reproduced with permission.[124] Copyright 2020, ACS. I) Effects of surrounding media on the LSP-induced temperature distribution of the ten-particle chain. Reproduced with permission.[125] Copyright 2010, APS.

that the higher the thermal conductivity of surroundings, the lower the transient temperature of the plasmonic nanostructure (Figure 10I). In this way, both the localized and collective heating effects can be completely utilized for the desired purposes by designing NP assemblies and/or thermal management realized via substrate engineering.

3.3. Combined Designs and Plasmonic Metamaterials

In real applications, a hybrid design that freely combines the abovementioned basic strategies is often adopted to achieve more desired performances. Irrespective of the way the materials and nanostructures are engineered, the ultimate objective is to achieve mutual coupling and overlapping of more resonant modes, and thus to both enhance and broaden the absorption performance. For instance, it has almost become a universal strategy to use plasmonic NPs with hybrid material designs,[131,132] wide-distributed sizes,[133,134] and/or various shapes[135] to achieve ultrabroadband absorption. These NPs supporting LSPs at selected wavelengths can be either suspended in solutions[136,137] or assembled on supporting substrates,[138,139] enabling ultrabroadband solar absorption and highly efficient photothermal conversion for targeted applications.

Another typical example is metamaterials, i.e., artificially structured materials with unit cells much smaller than the light wavelength of interest, which are termed meta-atoms.[140] These metamaterials enable significant flexibility in manipulating EM waves, producing new functionalities transcending those of natural materials.[48] However, plasmonic metamaterials offer higher flexibility by exploiting the highly tunable SPs. With respect to the utilization of solar energy, plasmonic metamaterials can be elaborately crafted to enable near-perfect broadband solar absorption[141–143] as well as spectrally selective thermal emission[144–148] favored.

Fundamentally, realization of an efficient solar absorber should simultaneously meet the demands of effectively absorbing light and then confining its energy inside the material. For any opaque material, maximization of its absorption requires elimination of the reflectance as much as possible. The reflection can be minimized by achieving the “impedance matching” with the free space,[149,150] which can be accomplished via making lattices,[151] gratings,[152,153] cavities,[72,154–156] or other nanostructures[157,158] to trap the air inside. In this way, the effective impedance of nanomaterials such as metals and semiconductors can be significantly reduced. However, for planar multilayered metamaterials, an antireflection layer is often required to reduce the reflection.[159] On the other hand, resonant excitations such as SPs enable strong confinement of the incident light energy inside or around the nanostructures. Plasmonic metamaterial absorbers based on NPs assembled on/in porous substrates, cermet-based multilayers, metal–insulator–metal (MIM) structures, and other similar structures are all typical examples, which are further discussed in detail in the following sections.

Following the light absorption, the photothermal conversion in plasmonic absorbers can be tailored via nanostructure-mediated thermal management. For example, a broadband perfect plasmonic absorber based on a trench-like thin metallic structure demonstrated superior photothermal performance, where the heat was effectively conducted through the continuous metal film, while barely dissipated via radiation in the MIR regime.[160]

4. Nanothermometry

The capability to measure local temperature changes in nanomaterials is critical for understanding the basic properties of thermoplasmonics. This calls for nanothermometry with sufficiently high spatial, temporal, and thermal resolutions.

Till date, substantial advances have been made to develop such a capability, and the reported techniques fall into the following three categories: contact techniques mainly based on scanning microscopy or microthermocouple technique (e.g., scanning thermal microscopy (SThM), etc.), noncontact optical techniques (e.g., IR thermography, Raman spectroscopy, thermoreflectance, interferometry, etc.), and semicontact techniques based on various luminescent NPs (e.g., organic dyes, proteins, quantum dots, nanodiamonds, and lanthanide-ion-doped NPs).[161] Each technique has not only its own unique strengths, but also distinct weaknesses. For example, SThM provides high spatial resolution (≈10 nm) and high sensitivity (≈10 mK);[162,163] nonetheless, it is often invasive and enables temperature detection only on the surface. Besides, it requires slow scanning to produce a thermal image and needs complicated equipment as well as rigid measuring conditions such as high vacuum, making it difficult for utilization in practical applications. By contrast, noncontact optical methods can be remotely used and often allow for the extraction of thermal information from not only the surface, but also inside the sample. This is particularly important for systems in biomedical, chemical catalysis, and other applications where nanoheaters are immersed in aqueous solutions. They often depend on the temperature-induced changes in the inherent properties of the materials or surroundings including the refractive index, density, viscosity, phase transitions, etc. However, they suffer from diffraction-limited spatial resolution, for which IR microscopy is within a few micrometers (**Figure 11**). Although it is possible to use UV light to increase the spatial resolution to ≈100 nm, further overcoming the diffraction limit requires other radically different approaches. For instance, by operating in the near field, the scanning near-field optical microscopy enables to achieve a spatial resolution down to ≈10 nm, determined by the tip size, through probing the thermally driven fluctuating EM evanescent fields.[164] For the last category, the luminescent-NP-based nanothermometry depends on the characteristic response to temperature, originating from their molecular-, atomic-, and even electronic-scale dynamics, which are phenomenologically measurable via various optical indicators, e.g., peak position, emission intensity, polarization anisotropy, lifetime, electron spin resonance, and optically detected magnetic resonance.[165] These techniques also enable remote sensing but require that the nanomaterial must be located in the illuminated area. Besides, their spatial resolution is also determined by the wavelengths of the light applied, just the same as the noncontact optical methods, and thus is also diffraction-limited due to the far-field detection in most cases. Therefore, apparently, all these techniques have their own features relying on the measuring principles and should be carefully selected for a specific application. One can find more detailed guidance by referring to several special reviews.[161,165–167]

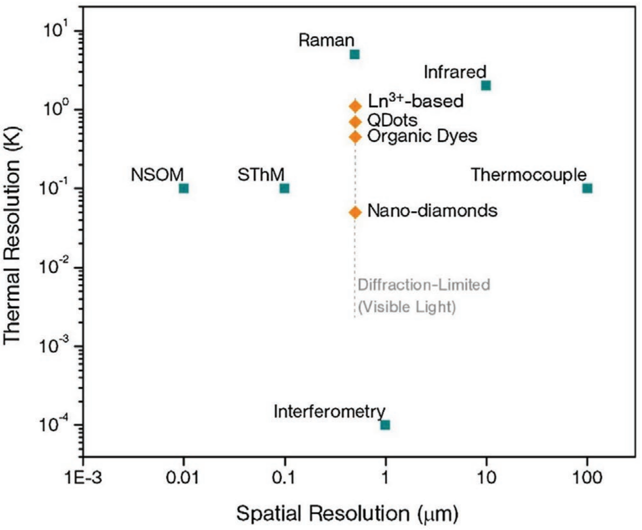

Figure 11. Typical thermal resolution versus spatial resolution for various thermometry techniques with sub-micrometric resolution. Reproduced with permission.[161] Copyright 2018, Elsevier.

The field of nanothermometry is still nascent, but rapidly evolving. A recent trend involves the development of techniques that enable high-temperature measurements as well as ultrahigh temporal resolution. Both are critical to understanding the nonlinear thermo-optical properties and ultrafast thermal dynamics in thermoplasmonics, and also indispensable to studying related dynamics such as the fast spatiotemporal distributions of heat generation and dissipation involved in practical biological, chemical, and physical applications. Lanthanide-doped inorganic nanomaterials, e.g., Yb^{3+}–Tm^{3+}-codoped YVO_4,[168] Yb^{3+}–Nd^{3+}-codoped La_2O_3,[169] etc., have shown significant potential to enable high-temperature measurements at temperatures above 1000 K, due to their weak thermal quenching effects at elevated temperatures. The use of time-domain thermoreflectance along with optical thermoreflectance imaging technique has recently managed to study the optical and thermal dynamics of plasmonic nanostructures with a spatiotemporal resolution in the nanometer–nanosecond regime.[170] Currently, some techniques have been applied in real-life situations; nonetheless their use is not extensive yet. Undeniably, a lot more systematic explorations are still demanded to carefully test these techniques under diverse conditions to guarantee their robustness and to facilitate them toward standardization.

5. Solar-Driven Thermoplasmonic Applications

As mentioned in Section 3, by finely tailoring their thermoplasmonic responses, it is possible to design nanostructures capable of interacting with the entire solar spectrum and beyond, thus deriving versatile and optimized solar energy applications.[171] Herein, the recent progress of solar-driven applications including solar evaporation, photothermal catalysis, and solar thermophotovoltaic (STPV) systems, where thermoplasmonics plays a critical role, are mainly focused upon.

5.1. Plasmon-Enhanced Solar Evaporation

Solar evaporation provides a promising platform for diverse applications such as seawater desalination,[157,172,173] distillation,[174] power generation,[157] wastewater treatment,[175,176] etc., to address the serious global challenges of water scarcity and energy production.[177,178] Till date, various integrated solar evaporation systems have been developed, in which solar irradiation can be efficiently absorbed and converted into heat, which is then utilized to generate steam. Tremendous research efforts have been devoted to exploring materials and nanostructured designs to obtain efficient solar absorbers. Two types of materials are commonly adopted: carbon-based and plasmonic materials. The former include carbon black,[179] graphite,[180] graphene oxides,[181] and many others[20] that enable broadband strong absorption attributed to their π–electron interband transitions and inherent black color. By contrast, plasmonic nanostructures have attracted tremendously growing attention due to their highly controllable performance.

In general, these plasmonic absorbers can be arranged into two systems, namely, volumetric (**Figure 12**A,B) and interfacial (Figure 12C) types. A volumetric system is often based on nanofluids, a type of colloidal suspension with plasmonic NPs stably dispersed inside water followed by its in situ heating. In this system, the design of single plasmonic NP is critical to enable broadband absorption. However, this approach inevitably results in bulk heating that leads to the increase in the heat loss and decrease in the solar-to-vapor conversion efficiency. In this context, an interfacial system stands out as it avoids bulk heating by localizing both the heat and evaporation at the water–air interface. It often involves large quantities of plasmonic NPs assembled on/in a variety of substrates that assist the improvement of both solar absorption and thermal management. Herein, recent advances in plasmonic absorbers are presented in terms of single NP designs as well as NP assemblies with substrates, and the related major challenges for future developments are summarized.

5.1.1. Single Nanoparticle Designs

For single plasmonic NP design, strategies including utilization of hybrid materials and/or elaboration of nanostructures are commonly adopted. For instance, nanofluids based on Au@SiO_2 core–shell NPs exhibited a higher efficiency than those based on carbon particles, due to the LSP-enhanced photothermal conversion. By further breaking the structural symmetry, the Janus NPs exhibited full-spectrum absorption due to the effective SP coupling among elementary geometries.[182] Besides, hollow mesoporous plasmonic nanoshells (HMPNs) of Ag/Au bimetallic system were systematically explored to yield a higher vapor generation rate than their solid-core counterparts (**Figure 13**A), due to the enhanced intracoupling effects, minimized scattering, and improved vapor dynamics.[183] Moreover, 2D MXene such as $Ti_3C_2T_x$ was also recently explored to synthesize hyperstable nanofluids.[98,184] The thin-layered $Ti_3C_2T_x$ NPs exhibited better photothermal performance than their multilayered counterparts due to both the SP coupling between flakes separated by tiny distance and the tip effect of its hexagonal shape.[184]

In case of nanofluids, the broadband solar absorption was achieved by blending a mixture of NPs with different SP resonances across the solar spectrum, such as blending of Au NPs with different NP sizes[133] or shapes,[135] and different material composites including Au/TiN,[71] Au/Ag,[185] etc.

Localized heating effects mediated by LSP can also be utilized to improve the energy conversion efficiency in plasmonic nanofluids. Although explanations regarding the underlying mechanisms for plasmonic-NP-mediated vapor generation have been debated over the past few years, this kind of volumetric absorbers can work in either a nonequilibrium or equilibrium manner relying on the degree to which the heat can be localized.[187]

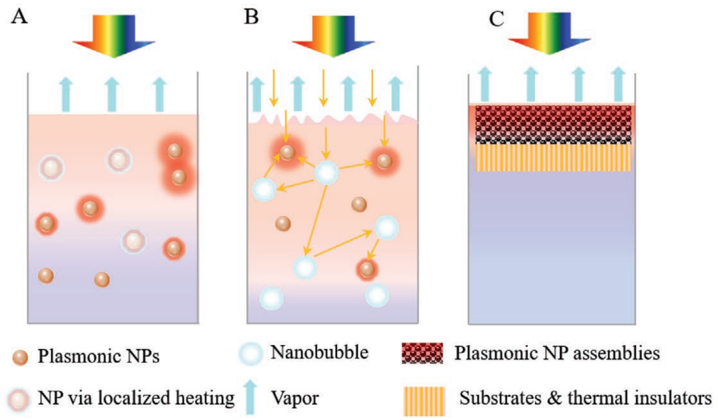

Plasmonic-enhanced solar evaporation

- **Broadband solar absorption**
  - ✓ Single Nanoparticle design: material, size, shape
  - ✓ NP assemblies: SPs coupling mediated
  - ✓ Optimization: Hybridizing diverse SP resonances
  - ✓ Substrates: increasing optical path/multi-photon scattering
- **Thermal insulation design**
  - ✓ Minimize heat loss
  - ✓ Localize heat and evaporation at the interface
  - ✓ Water supply

Figure 12. The schematic illustration for different evaporation systems: A) classical nanofluid based on plasmonic NPs; B) bubble-flow-driven nanofluid to enhance absorption, while reducing the usage of NPs; and C) interfacial evaporation based on plasmonic NP assemblies deposited on porous substrates.

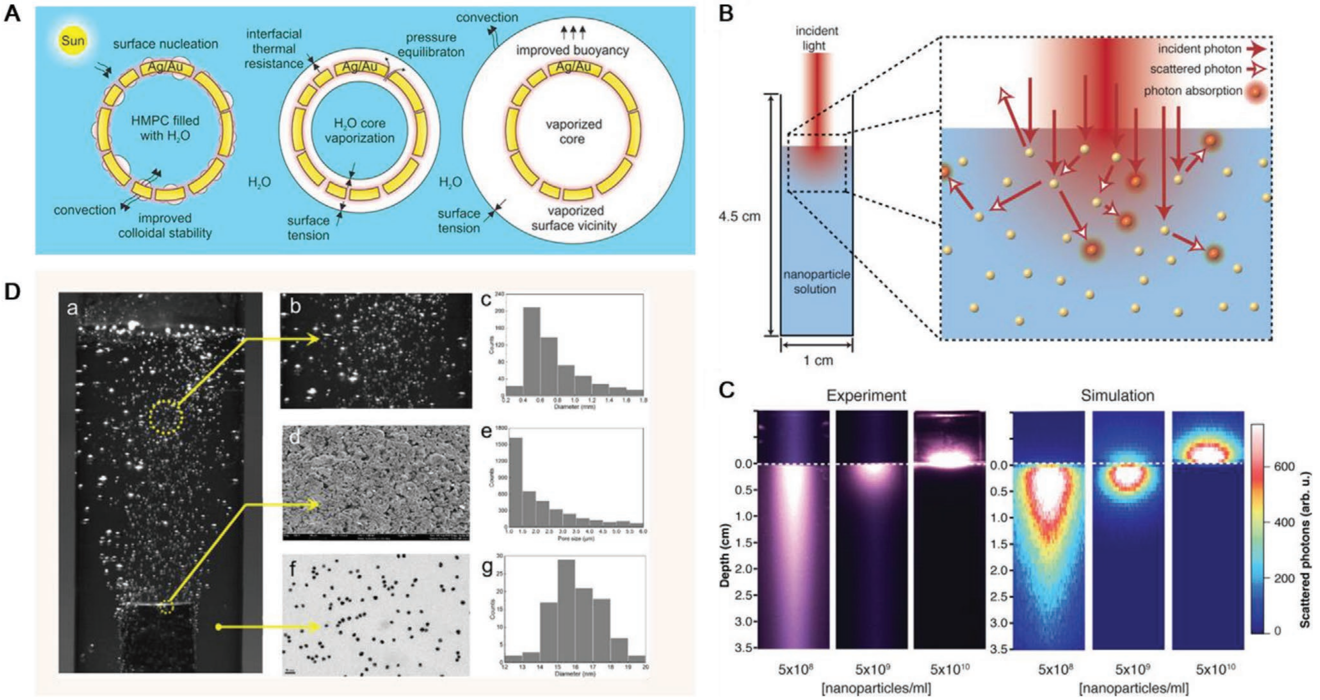

Figure 13. Plasmonic NP designs for volumetric evaporations. A) Schematic illustration of HMPN for enhanced solar vapor generation and the underlying mechanisms. Reproduced with permission.[183] Copyright 2016, ACS. B,C) The light-scattering properties of plasmonic-NP-based nanofluids: (B) schematic representation of the multiparticle optical interactions that help promote the scattering and/or absorption of incident photons; (C) experimentally obtained (left) and Monte Carlo simulated (right) scattered light as a function of NP concentration. Reproduced with permission.[186] Copyright 2014, ACS. D) Photos for the as-designed bubbly flow nanofluid system and size distributions for the bubble swarm, bubble generator, and Au NPs. Reproduced with permission.[193] Copyright 2020, Elsevier.

For the former, the suspended plasmonic NPs enabled the confinement of heat in the space very near the particle–liquid interface in a nonequilibrium manner. In this case, the NP gets heated up to a temperature sufficient to nucleate a vapor bubble locally, while the surrounding bulk water remains cold. For instance, the SiO_2 shell of the plasmonic Au@SiO_2 core–shell NPs can help to localize the heat and yield a significantly higher photothermal conversion efficiency than that of carbon particles, due to less heating of the bulk liquid.[188] Furthermore, microscopic mechanisms have also been explored.[188,189] For the latter, NPs rapidly reach thermal equilibrium with the surrounding water, and the vapor is generated as a direct result of the increase in the bulk temperature.[187] Experimental results indicated that the LSP excitation of a single Au nanowrench could result in the superheating of water to about 600 K before bubble formation,[190] which distinctively differed from the colloidal Au NP solution where collective heating effects dominated and led to the boiling of the solution exactly at the boiling point. Noteworthy, several factors should be carefully determined to achieve these two distinct heating conditions including the absorption and scattering properties of the NPs, the NP concentration, the incident light power intensity, and others (Figure 13B,C).

Next, the change of surroundings can also distinctively alter the overall photothermal performance of these volumetric absorbers. For example, introduction of dynamic bubbles into plasmonic nanofluids, termed as bubbly flow nanofluids,[191–193] can further improve the steam generation. These bubbles can act as optical scattering centers that extend the path of incident light and thus increase the absorbed solar flux. The results showed a 3 times higher evaporation rate for Au-NP-based nanofluids with a very low concentration than that of pure water (Figure 13D).[193] Better performance can be expected by increasing the light intensity, NP concentration, and gas flow rate.

When it comes to the interfacial system, single NP design is also significantly important. Numerous plasmonic NPs with well-designed nanostructures, including black Ag nanostructures,[138] Au nanotrepangs,[194] Au flowers,[107] Ag–polydopamine core–shell NPs,[195] etc., have been demonstrated. However, to localize both the heat and evaporation at the water–air interface, these NPs have to be appropriately assembled on/in substrates, together with thermal insulators, to yield higher evaporation efficiencies.

5.1.2. Nanoparticle Assemblies with Substrate Designs

In the interfacial system, plasmonic NPs are often carefully assembled on/in porous substrates to act as solar absorbers, with a porous thermal insulator integrated beneath to reduce conductive heat loss downward (Figure 12C).[196] The entire system is made lightweight to enable self-floating on the water/air interface and thus the interfacial evaporation. Till date, solar-to-steam efficiencies higher than 90% have been successfully achieved by exploring new materials and nanostructured designs.[197,198]

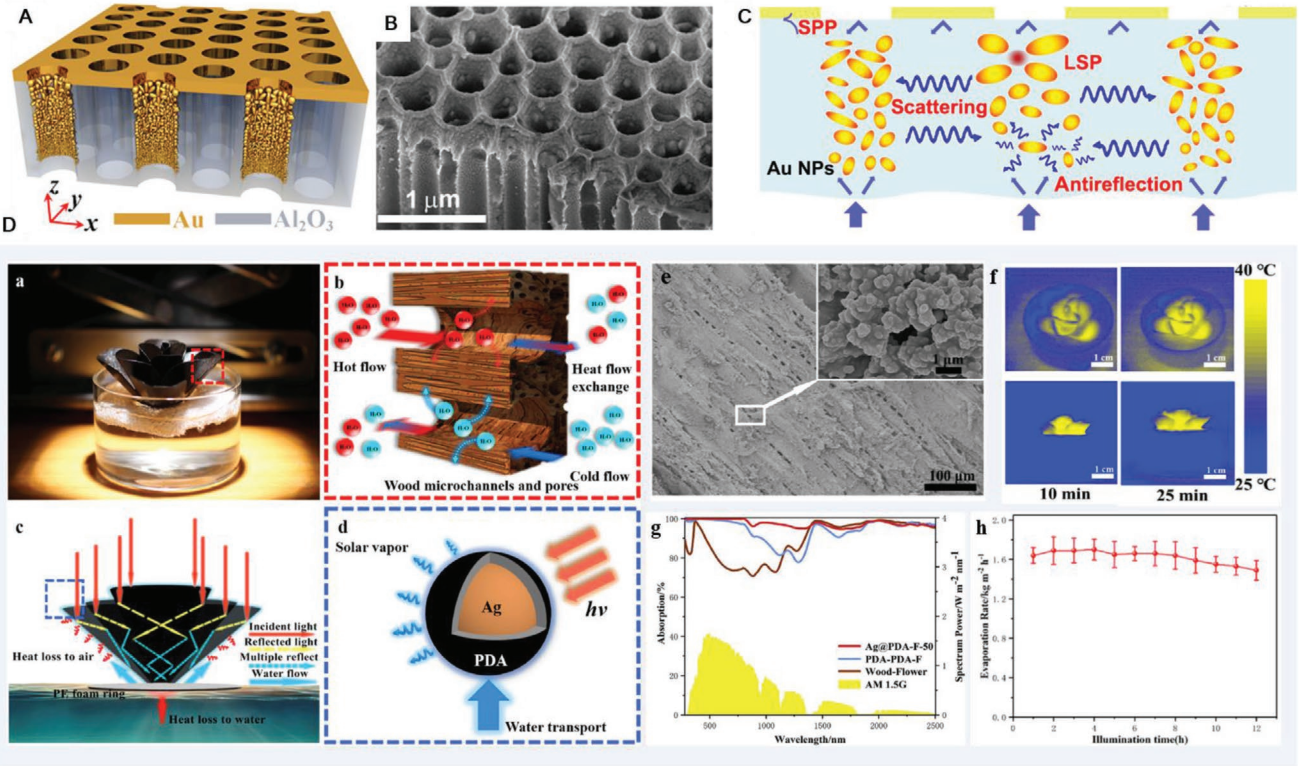

Figure 14. Demonstrations of solar-driven interfacial evaporation systems: A–C) Au NPs densely deposited in 3D porous substrate: (A) schematic illustration and (B) SEM image of the fabricated evaporation structure; (C) schematics showing the underlying mechanisms;[129] D) 3D wooden lotus flowers decorated with plasmonic Ag@PDA core–shell NPs: a) photographs of the fabricated 3D wooden flowers; b–d) the underlying mechanisms; e) SEM images of NPs deposited on the flower surface; f) heat distribution and localization via thermal IR camera; and g,h) measured absorption and evaporation rate. Reproduced with permission.[195] Copyright 2020, Elsevier.

Similar to the volumetric system, coupling effects of LSPs can also be effectively employed to enhance the solar absorption. The plasmonic NPs with distributed sizes and/or various shapes have been assembled into aggregates, porous, or even more complex structures.[197,199] For instance, Au and Ag NPs with different sizes were, respectively, deposited on both the top surface and sidewalls of a 3D porous template to form plasmonic absorbers (**Figure 14**A,B).[129,139] These self-assembled plasmonic NPs enabled the individual LSP modes to overlap and hybridize with each other, resulting in broadband absorption and strong collective heating effects. Moreover, the 3D porous template also plays an important role in enhancing absorption via strong internal trapping effects, which leads to significant increase in the optical path lengths as well as reduction in reflection due to the relatively low effective refractive index (Figure 14C).[200,201] In this case, ultrabroadband (300–2500 nm) and near-perfect absorption (>95%) were achieved, and thus highly efficient desalination (≈90%) was also attained.

Significant research attempts have also been made for exploring new plasmonic materials, optimizing assembled NPs, and improving porous evaporation structures. For materials, Al NPs have been adopted to alternate noble metals to reduce cost and to improve stability due to the thin oxidation passivation layer;[128] semiconductor crystals such as CuS NPs have been investigated due to their near-IR absorption and easy fabrication;[202] and TiN has also been explored due to its low cost and high-temperature stability. For instance, a scalable ultrathin solar absorber based on TiN nanocavity arrays with thickness down to 250 nm was fabricated that yielded a solar absorption of 90% and an evaporation efficiency of ≈76% at 14 suns.[203] This kind of quasi-2D metasurface enables to minimize the amount of required material and maximize the heat power density within the ultrathin absorbers themselves, thus reducing the material cost while promoting rapid thermal and evaporation dynamics that boost the system efficiency.[203] However, for the substrate design, the pore sizes, wettability, and density are all important factors to be considered. Artificial porous materials including carbon cloths,[175] foams,[204] aerogels,[194] polymers,[205] papers,[206] etc., and natural materials with inherent microchannels and low thermal conductivity, e.g., wood,[207] bamboo,[208] etc., have been adopted to allow for good water transport and heat localization. The latter is crucial for interfacial evaporation under low optical concentration, for which the realization necessitates four structural characteristics including absorption across the solar spectrum, thermal insulation, hydrophilic behavior, and interconnected pores.[209] For example, a plasmonic interfacial absorber based on 3D wooden lotus flowers decorated with plasmonic (Ag@polydopamine (PDA) core–shell) NPs was recently demonstrated to achieve a light absorption of 98.65% within 280–2500 nm and a solar-to-vapor efficiency of 97.0% under 1 sun (Figure 14D).[195] In this case, a thermal insulator made of polyethylene foams was also inserted beneath the wooden flower, which enabled thermal concentration and thus continuous evaporation. This thermal concentration concept paves the way to design a solar-driven evaporation system without optical concentrators, which might lead to significant decrease in the cost of interfacial steam generation systems.[131,210]

Though promising as it is, further research efforts are still required to be devoted to improve the efficiency under one sun, namely, eliminating the optical concentrators to make this technology more cost-effective. Other challenges toward practical applications include the integration of this interfacial evaporation system in commercial cycles, operation under transient and real working conditions, long-term stability of the material, nanostructures, and systems, all of which require further systematic explorations.

5.2. Plasmonic Photothermal Chemistry

Light and heat are important physical quantities that control chemical transformations. The rate constant K of most chemical reactions follows the Arrhenius law: $K \propto \exp(-E_a/RT)$, where T is the temperature, E_a denotes the molar activation energy, and R is the gas constant. The use of plasmonic nanostructures can boost the reaction rates due to the increase in the local temperature, along with the optical near-field enhancement and hot-carrier generation.[211] These functionalities make plasmon-enhanced photothermal catalysis very attractive and drive its growth into an extensive research area, as it can contribute to nanoscale synthesis, clean energy production, and many other useful fields.

Thermoplasmonics mainly studies the photoinduced localized/collective heating in plasmonic materials, and in this sense, hot-carrier effect is indeed not the process of interest in this review. However, for plasmonic photothermal catalysis, Ozin and co-workers stated that hot carriers and the heating effect contributed synergistically to the enhanced overall reaction rate, with both mechanisms playing a vital role to various degrees depending on the operating system.[212] Gascon and co-workers also included both mechanisms into the study scope of plasmonic photothermal catalysis and considered that it arose from the combination of both thermo- and photochemical contributions of nonradiative plasmon decay.[213] The fact is that these two mechanisms are so tightly entangled that distinguishing them from each other has become one of the most challenging research hotspot in this field,[73,214–216] as they occur on timescales broadly overlapping with the time constants of typical chemical reactions.[124] This is also the reason why the field of plasmonic hot-carrier chemistry experienced heated debates regarding the actual underlying mechanisms even after decades of extensive activities.[21] For these reasons, the remaining part of this section is divided into the following two parts: the first part briefly introduces thermoplasmonic-assisted synthesis where often plasmonic heating is the targeted process. The second part aims at plasmon-enhanced photothermal catalysis toward solar energy utilization, where both mechanisms may play a dominant role.

5.2.1. Thermoplasmonic-Assisted Synthesis

Thermoplasmonics plays an important role in photothermal chemistry because it provides controlled nanoscale thermal environments. Compared to regular heating techniques such as using a hot plate, the most distinct advantage of this plasmonic heating is that it offers spatial confinement that enables precise control over the growth, assembly, and patterning of nanomaterials. Besides, this localized heating can yield a large temperature rise under moderate illumination intensity, which potentially makes the process more energy efficient by avoiding bulk heating. Moreover, it may also contribute to improving the catalytic activity of some plasmonic NPs, which is often temperature-dependent. All these merits offered by thermoplasmonics render it a promising approach for the synthesis of advanced materials with tailored functionalities, giving rise to the field of thermoplasmonic-assisted synthesis. The potential of this field has already been highlighted in numerous literature studies, where the chemical growth reactions could be selectively triggered with high spatial resolution.[217,218]

For instance, plasmonic-assisted chemical vapor deposition (PACVD) enables site-specific heating of the substrate with light and spatially controlled growth of targeted nanomaterials by using plasmonic metal NPs as both catalysts and nanoheaters. This approach was first reported in 2006 and demonstrated the micropatterning of PbO and TiO_2 on glass substrates coated with Au NPs by using a focused low-power laser.[217] Then in 2007, PACVD with a subdiffraction resolution was also successfully achieved and demonstrated highly spatial and temporal control over the growth of semiconductor (Si, Ge) nanowires and CNTs by locally heating the Au catalysts with light in room-temperature chambers.[218] This local heating strategy has been demonstrated to be several orders of magnitude ($>10^5$) more energy efficient compared to the conventional CVD tools where the entire chamber/substrate is heated.[218] Thereafter, this technique developed very rapidly and extended to one-pot synthesis of nanomaterials in the liquid phase.[219,220] Very recently, the conformal growth of semiconducting shells, including CeO_2, ZnO, and ZnS, around plasmonic NPs with different morphologies was demonstrated in the liquid phase by exploiting the LSP-mediated local temperature gradients.[220] The shell growth was well-controlled with tunable chemical compositions and thickness down to approximately nanometer scale.[220] Notably, even though photoinduced plasmonic localized heating is often the targeted process in these thermoplasmonic-assisted syntheses, other mechanisms such as the electric and magnetic dipole resonance and hot carriers may also contribute to the catalytic growth of these NPs. Distinguishing among all these possible activation mechanisms is always a challenging task, but can definitely be realized via elaborated approaches. For instance, by using appropriate experimental approaches together with FDTD simulation, the transfer of interband holes to ascorbic acid was identified as the major mechanism that limited the growth rate of the Ag shell in the synthesis of plasmon-assisted Au@Ag core@shell nanorods.[221] Another picture to use thermoplasmonics is to drive physical phase transformations such as melting, welding, etc., of nanomaterials to achieve subdiffraction nanofabrication. For instance, plasmonic NPs with arbitrary morphologies can be reshaped into nanospheres by reducing their sharpness, such as the gradual rounding of Au triangular NPs,[222] as these sharp points are often the spots where the LSP-induced thermal hotspots locate and the melting initiates. Besides, self-limited nanowelding of Ag nanowires was achieved at the junction points by utilizing this highly localized heating, which yielded a size resolution down to ≈50 nm.[223] These techniques offer alternative nanofabrication methods to the currently employed expensive electron beam lithography (EBL) and focused ion beam (FIB) due to the scaling-up potential.

However, it is difficult to use solar energy as the light source in these syntheses, because monochromatic lasers are often required, with a wavelength coinciding with the required LSP resonance, a highly focused spot size, and a well-controlled intensity, to ensure precise thermal control. Therefore, more emphasis is put on plasmon-enhanced photothermal catalysis toward solar energy utilization in the following section.

5.2.2. Solar-Driven Plasmonic Photothermal Catalysis

Photocatalysis that directly converts solar irradiation into chemical products has been extensively studied in various applications such as water splitting,[106,224] CO_2 conversion,[225,226] pollutant degradation,[227] etc. However, traditional photocatalysts such as semiconductors and metal complexes generally suffer from low efficiency due to their limited light absorption and rapid electron–hole pair recombination.[23] Plasmonic NPs have recently emerged as promising complements due to their aforementioned fascinating functionalities. Besides, plasmonic catalysis enables catalysis of reactions under conditions much milder than those involved in traditional thermal catalysis, thus avoiding the exorbitant energy requirements. In this sense, plasmonic photothermal catalysis synergistically combines the photo- and thermo-chemical contributions of sunlight. Given these features, it is thus necessary to develop efficient plasmonic nanocatalysts with well-designed architectures to harness the full potential of photothermal conversion. These plasmonic photothermal catalysts should meet several requirements including a strong and full-spectrum light absorptivity, an efficient generation and separation of hot carriers, and a high capacity for heat generation. In the following section, strategies to design plasmonic photothermal catalysts are outlined in terms of single catalysts with hybrid architectures and assembled catalysts with hierarchical constructions.

Single Catalyst with Hybrid-Architecture Design: Importantly, the material and structural designs of single nanocatalysts direct the physical properties underlying the photothermal effect. Plasmonic metals such as Au,[228] Ag,[229] Cu,[54] Al,[230] etc., can drive photothermal catalytic processes by offering dual functions, i.e., both plasmonic and catalytic. For instance, it was demonstrated that Au NP catalysts effectively favored the steam reforming of ethanol when illuminated with a low-power laser, where the plasmonic heating provided the necessary heat for the reaction that resulted in local vapor generation over them.[231] In this pioneered study, the underlying mechanism was clarified by visualizing and monitoring the evolution of bubbles.[231] Besides, Au core/porous shell NPs were synthesized, which demonstrated higher catalytic efficiency than other reported Au nanostructures due to the highly porous shell and hollow structures that enabled LSP-mediated enhanced absorption and improved transport of hot electrons.[232] However, this type of single-component plasmonic catalysts suffer from drawbacks such as limited light absorption, poor tunability, etc., and are suitable for only a very few chemical processes.[233]

By contrast, a hybrid configuration offers advantages with respect to the optical, electronic, structural, and chemical properties of the two materials, instead of just one.[212] For instance, the combination of plasmonic NPs with traditional catalysts integrates the photon-harvesting and catalytic abilities into single multifunctional architecture, and thus diversified surface chemistry and reactivity are not achievable for single-component nanostructures. One versatile strategy of this hybrid design is the antenna–reactor (A–R) complexes,[233–235] in which the plasmonic NPs act as nanoantennas to enhance the light absorption, and thus promote the transfer of both hot carriers and heat to the active sites on the reactors. Interestingly, this strategy is a highly modular one such that both the plasmonic antenna and catalytic reactor can be tailored by varying the compositions and/or nanostructures.[235] Several examples of the possible hybrid architectures are illustrated in **Figure 15**, where the catalytic reactors can be placed close to (e.g., heterometallic dimers), adhered to (e.g., multicomponent heterostructures), or even wrapped around (e.g., core–shell heterostructures) the plasmonic nanoantennas. Both the components can be separately tuned by their sizes, shapes, relative positions, and even distributed densities, thus the desired catalytic performance can be achieved.

In general, the A–R hybrid designs have shown catalytic efficiencies much higher than those of their single-component counterparts. For instance, bimetallic plasmonic catalysts

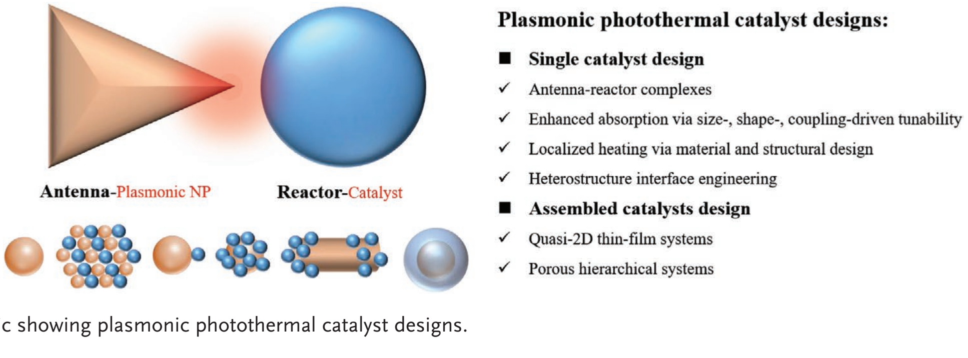

Plasmonic photothermal catalyst designs:

- **Single catalyst design**
  - ✓ Antenna-reactor complexes
  - ✓ Enhanced absorption via size-, shape-, coupling-driven tunability
  - ✓ Localized heating via material and structural design
  - ✓ Heterostructure interface engineering
- **Assembled catalysts design**
  - ✓ Quasi-2D thin-film systems
  - ✓ Porous hierarchical systems

Figure 15. Schematic showing plasmonic photothermal catalyst designs.

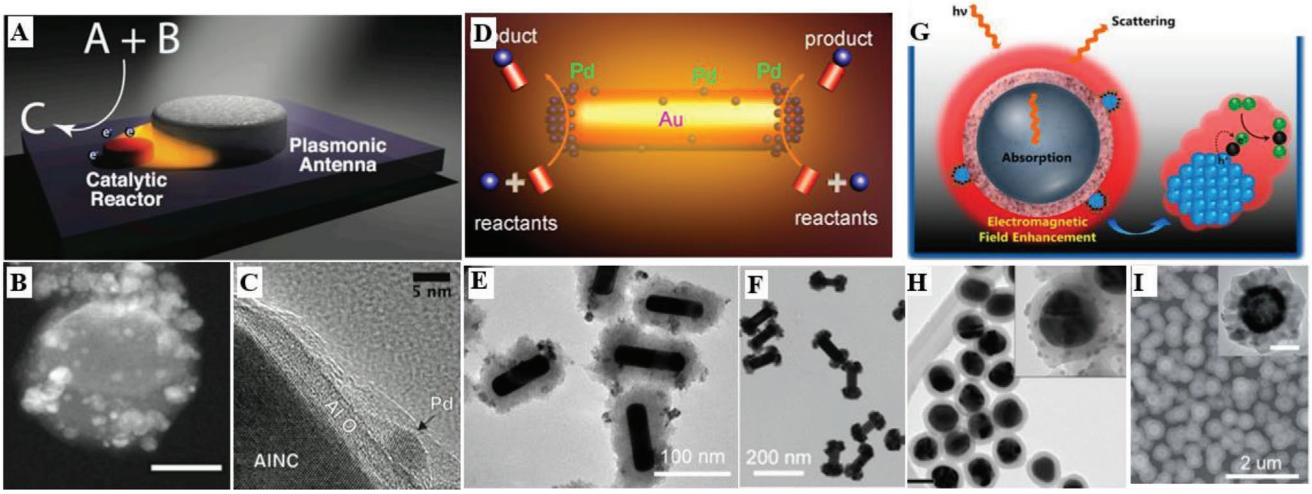

Figure 16. Hybrid antenna–reactor configurations. A–C) Al–Pd heterodimers: (A) schematic illustration; (B,C) SEM images of Pd-decorated Al NCs. Reproduced with permission.[234] Copyright 2016, ACS. D,E) Pd-NP-decorated Au nanorods: (D) schematic illustration and (E) SEM image. Reproduced with permission.[236] Copyright 2013, ACS. F) transmission electron microscopy (TEM) image of Au/end-CeO_2 nanostructures. Reproduced with permission.[243] Copyright 2019, ACS. G–I) Core–shell structural designs: (G) schematic representation; (H) SEM and TEM (inset) images of Ag@SiO_2/Pt heterostructures. Reproduced with permission.[244] Copyright 2017, ACS. I) SEM and TEM (inset) images of Cu_7S_4@ZIF-8 NPs. Reproduced under the terms of the CC BY license.[240] Copyright 2016, The Authors. Published by The Royal Society of Chemistry.

based on multiple small-Pd-island-decorated Al NCs were synthesized to drive catalytic hydrogen dissociation (HD) (**Figure 16**A–C).[233] The plasmonic Al antenna enhanced the local light absorption, promoted the hot-carrier-induced desorption, and aided in heating the active surfaces on the Pd reactor, thus leading to HD almost two orders of magnitude higher than that of the pristine Al NCs.[233] Besides, Pd-decorated Au-nanorod-end heterostructures were synthesized to catalytically drive Suzuki coupling reactions, where the contributions of plasmonic photocatalysis and photothermal heating were ascertained to the reaction yields (Figure 16D,E).[236]

Although singling out the dominant mechanism for a specific reaction remains a challenging task, some clues can still be outlined to design these plasmonic nanocatalysts toward enhanced photothermal conversion. Regardless of the dominant mechanism, materials with delicate architectures enabling broadband near-unity solar absorption are expected to promote both the hot-carrier and heat generation, and thus lead to optimized photothermal catalytic performance. For instance, photothermal catalysts based on In_2O_{3-x}/In_2O_3 heterostructures were synthesized to drive the photothermal reverse water gas shift reaction under ambient conditions with 100% selectivity.[237] By controlling its nonstoichiometry degree, the nanocatalyst achieved full-spectrum strong solar absorption due to its black color and high surface area and thus provided an excellent photothermal performance. The strong local heating in the In_2O_{3-x}/In_2O_3 heterostructure effectively catalyzed the thermochemical hydrogenation of CO_2; while the LSP-induced hot carriers promoted the photochemical reduction of CO_2. These two beneficial effects synchronously worked and resulted in this excellent catalytic performance. In this sense, design strategy benefiting the improvement of the light absorption may accordingly contribute to the optimization of the photothermal catalysis, which can be realized by exploiting the size-, shape-, and coupling-driven tunability of LSPs.[238]

A hybrid architecture composed of materials with large inherent loss may contribute significantly to enhancing the photothermal conversion and related catalytic activity. For instance, a model system was proposed by depositing a catalytic shell with a large ε_2 (e.g., Pt) on a core plasmonic NP with a significantly lower ε_2 (e.g., Ag), which aimed at controlling the energy flow for catalytic processes.[239] The introduction of a 1.2 nm thick Pt shell onto an Ag cube core led to significant enhancement in the light absorption property and directed the selective dissipation of LSP energy through these Pt sites, due to its larger inherent loss. It was further postulated that this selective LSP-induced energizing of the Pt active sites ultimately led to the selective heating of the most-abundant reaction intermediate (CO) on the catalyst surface, which finally resulted in elevated reactions rates.[239]

Hybrid architecture designs favoring localized heating, such as core–shell structures by enwrapping plasmonic NPs with thermal insulators, are expected to benefit the improvement of the photothermal catalytic activity. Materials with high porosity and large surface areas such as metal–organic frameworks (MOFs) or covalent organic frameworks (COFs) are particularly desirable. In general, their porous structures possess very high specific surface areas featuring enriched catalytic active sites and intermolecular interaction. Besides, they often exhibit low heat conductivity and are inherently structurally predesignable for targeted catalytic reactions. All these merits make them unique for this hybrid catalyst design. For instance, Au&Pt@zeolitic imidazolate framework (ZIF) hybrid nanocatalysts were synthesized for CO_2 hydrogenation, with Pt nanocubes and Au nanocages encapsulated in a ZIF-8.[114] The Au nanocages enabled LSP-enhanced light absorption and photothermal conversion, and Pt nanocubes provided catalytic active sites, while the MOFs functioned as thermal insulator to generate high local temperatures. Consequently, the catalytic activity of Pt nanocubes was greatly improved and the required reaction temperature was largely reduced.[114] Besides, a MOF-shell-encapsulated Al NC heterostructure (Al NC@MIL-53) was recently demonstrated to increase the catalytic efficiencies of both the hydrogen–deuterium exchange and reverse water–gas shift reactions.[60] Similar structures including hierarchical Cu_7S_4 hollow microspheres coated with ZIF-8 (Figure 16I),[240] Au–Ni alloy@MIL-101,[241] Au(Pd)@porphyrin-containing homochiral covalent organic framework (CCOF)–CuTPP,[242] etc., have also been explored. This approach can be universally extended to combine any plasmonic NPs or A–R complexes with MOF/COF shell layer, and thus it shows tremendous potential to benefit various photothermal chemical reactions.[184] From the application perspective, it is expected that this strategy can be used to construct a localized high-temperature environment under industry-favored ambient conditions, thus facilitating the practical conversion of solar energy to chemical energy.

The interfacial property of these A–R heterostructures is very crucial in determining the photothermal conversion because it dictates the transport of both heat and hot carriers. The formation of interfaces between two materials can improve the separation and lifetime of photogenerated carriers; however, the interfacial state including the surface defects, roughness, disorders, etc., strongly impacts the phonon transport and thus the interfacial thermal conductivity.[245] In this respect, it is necessary to improve the control over the interfacial properties when designing plasmonic catalysts. Semiconductor–metal heterocatalysts with Schottky junctions, such as Au/end-CeO_2 nanostructures (Figure 16F),[243] Au-NP-loaded hierarchical hollow porous TiO_2 spheres,[246] etc., have been synthesized to suppress the recombination of charge carriers and thus improve the related catalytic efficiencies.[173,243] In these designs, good alignment of the Fermi level of the plasmonic NPs with the bands of the semiconductors should be established to allow efficient carrier injection.[247] On the other hand, reduced thermal conductivity can be achieved by increasing the boundary scattering of carriers, which thus increases local temperature gradients at nearby active sites. However, recently obtained ultrafast spectroscopy results indicated that the extraction of one type of carriers (e.g., holes) resulted in a lower thermalization temperature and thus lower peak energy of the other type (e.g., electron).[248] Similarly, decreasing the size of the plasmonic component renders it efficient nanoheaters due to both the enhanced absorption and reduced thermal conductivity; nonetheless, it leads to poor charge carrier separation due to spatial confinement. An overall strategy should be considered when designing and optimizing plasmonic photothermal catalysts, as improving one property might negatively impact other properties. For instance, it has been demonstrated that a detailed balance of local field enhancement, scattering, and absorption for each component had to be struck in core@shell/satellite (Ag@SiO_2/Pt) catalysts to achieve optimal catalytic performance (Figure 16G,H).[244] Thus, it is of great significance to understand how the number, size, distribution, and other aspects of the nanoheaters and reactors influence both the catalytic activity and selectivity for a particular product. This is a very challenging task in terms of both experimental implementation and mechanism interpretation, due to these diverse effects that synergistically contribute to the observed catalytic performance.

Assembled Catalysts with Hierarchical Construction: Plasmon-mediated photothermal catalysts can drive chemical reactions under milder conditions, providing valuable platforms for large-scale solar-driven photothermal chemical processes once well assembled. The way that these nanocatalysts are assembled directly affects the light absorption, photothermal conversion, and overall catalytic performance.

One major concern when considering large-scale assembled catalysts is how to increase the overall solar energy harvesting. For black photothermal catalysts enabling full-spectrum absorption, the light penetration capability in the catalysts is restricted by their high-optical absorption strength, which thus limits the locations of active sites to within micrometers of the catalyst surface.[212] By arranging these catalysts into nanostructured 2D metasurface, the solar energy harvesting can be greatly enhanced, attributed to the strong LSP-mediated energy confinement that enables customized ultrathin plasmonic-based layers (≈100 nm) to absorb most energy of the solar spectrum. For instance, thin films of refractory plasmonic TiN cylindrical nanocavities manufactured via scalable process were employed for high-temperature heterogeneous catalysis, yielding a broadband absorption of 95% across the solar spectrum and a high local temperature of above 600 °C under moderately concentrated solar irradiation (**Figure 17**A,B).[249] The effective coupling between the cavity and LSP modes of the TiN nanofurnaces together with the optical loss of TiN was confirmed as the main mechanism underlying this excellent photothermal property. Despite the advantages of this type of 2D nanostructured thin film system in terms of enhancing solar energy harvesting, it necessitates the use of very large photoreactors that would be highly demanding in land use if enlarged to the industrial scale.[212]

In this sense, 3D hierarchical structures, such as macroporous foam monoliths, aerogel, gel, and other nanostructures with ordered or random pores, would be more preferable to have these photothermal catalysts assembled. Since their 3D porous hierarchical constructions provide an ideal platform to allow for the customization of catalytic, optical, thermal, and mass transport properties. For instance, a 3D porous photothermal catalytic (PTC) gel has recently been engineered with TiO_2/Ag nanofibers assembled to drive concurrent photothermal-enhanced solar desalination and photocatalytic hydrogen generation (Figure 17C).[250] In this design, the open 3D porous PTC gel enabled these photothermal catalysts to be directly exposed to light, thus circumventing the possible light-shielding effects of upper NPs and poor light penetration in the suspension systems. Besides, the aligned pores of the gel system not only offered an anisotropic thermal conductivity that warranted an effective confined interfacial heating, but also provided direct vapor and gas pathways that significantly enhanced the resultant yields. Importantly, this configuration offers an exemplified model system for hierarchical design to simultaneously achieve excellent optical and catalytic performance as well as multiscale heat and mass transport management capability. More notably, by complementing nanoscopic localized plasmonic heating with macroscale thermal confinement simultaneously, the photothermal conversion was largely optimized.

Noteworthy, when photothermal catalysts are assembled into large arrays, overheating or even damage of the nanostructures caused by collective heating effects may become troublesome.

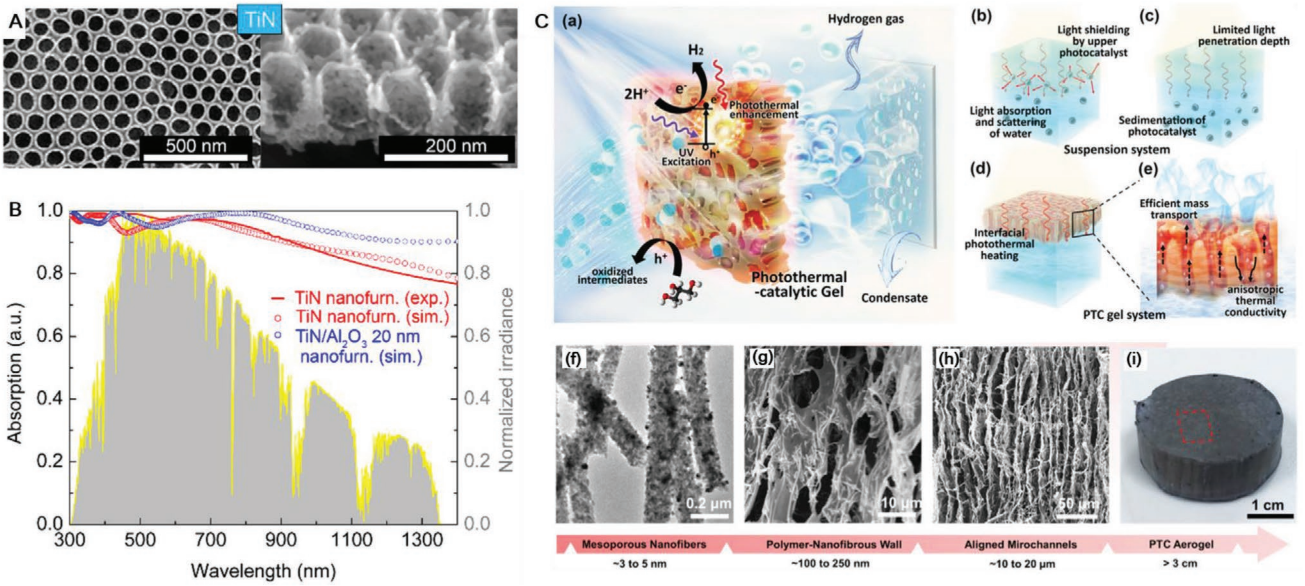

Figure 17. Typical assembled hierarchical structures of plasmonic photothermal catalysts. A,B) Thin-film system: (A) SEM images showing top and cross-sectional views of TiN nanofurnaces; (B) absorption spectra of TiN nanofurnaces. Reproduced with permission.[249] Copyright 2020, ACS. C) 3D porous PTC photothermal gel for concurrent solar vaporization and hydrogen generation: a) schematic illustration of the working principles for the designed PTC gel; b–e) distinct advantages of heat and mass transport properties of this PTC gel over traditional suspension systems; f) TEM image of TiO_2/Ag nanofibers; and g–i) SEM images of the fibrous wall of the PTC gel and its aligned microchannels. Reproduced with permission.[250] Copyright 2020, Wiley.

This is an important issue that must be considered for any large-scale thermoplasmonic applications. Very recently, by supporting the 3D A–R nanocatalysts on an insulating substrate within the antenna gap while the antenna maintained direct contact with an underlying thermal conductor, this issue was successfully eliminated.[251] Consequently, large nanoscale thermal gradients were achieved by maintaining large local temperature rises in the confined reactor, while minimizing the temperature rise of the surrounding antenna.[251] This nanostructure-mediated thermal management strategy is expected to be useful for applications such as small-volume, high-throughput chemical processes.

The plasmon-enhanced photothermal catalysis described herein provides an attractive opportunity to harvest and convert solar energy, and thus store it in the form of chemical energy. However, many challenges posed by the design and synthesis of nanocatalysts, underlying structure–activity relationship, light and heat management in large-scale assemblies, photoreactor engineering, process optimization, etc., still remain to be tackled carefully.

5.3. Solar Thermophotovoltaic

STPV has attracted tremendously growing interest due to their very high theoretical solar-to-electricity conversion efficiency of 85%,[252] which is about 2 times higher than the counterpart of standard PV cells known as Shockley–Queisser limit (≈41%). The low efficiency for the latter stems from the dispersed solar photon energy. This result is attributed to the fact that only bandgap energy contributes to the generation of electron–hole pairs, with the above-bandgap excess energy dissipating into heat while below-bandgap energy being totally lost. Multi-bandgap PV cells were proposed to overcome this efficiency limit; nonetheless, they turned out to be expensive and the heating problem remained unsolved.[253] In this context, TPV emerges as a promising alternative because of its capability to enable full-spectrum solar absorption and it also eliminates the heating issue by harvesting and converting all solar photonic energy into heat.

In general, a TPV consists of the following three key components: a solar absorber that converts solar energy into heat, a thermal emitter that emits heat as IR radiation, and a PV cell that converts the IR emission into electron–hole pairs, which are then captured to produce current (**Figure 18**). The key to obtaining an efficient TPV lies in the implementation of a solar absorber capable of strong broadband solar absorption and a thermal emitter allowing narrowband emission that enables spectral match with the PV bandgap. In both cases, plasmonic nanomaterials can play an important role. Notably, the working temperature of TPV is determined by the bandgap of PV cells with a low value in the range of about 0.8–1.1 eV.[21] This requires the emitter temperature to be between 1000 and 2000 K, which significantly restricts the choice of possible materials. Besides, this high operating temperature also exerts higher demands on solar absorbers in TPV than those in evaporation, because radiative heat loss becomes dominant and thus has to be minimized toward improved efficiency. At this point, selective solar absorbers are more desirable than the blackbody-based ones because they enable both broadband solar radiation (250–2500 nm) absorption and thermal radiation suppression within longer wavelengths (>2500 nm) at high temperatures.[254]

This section focuses on the recent advances on various selective absorbers/emitters toward TPV applications (**Figure 19**),

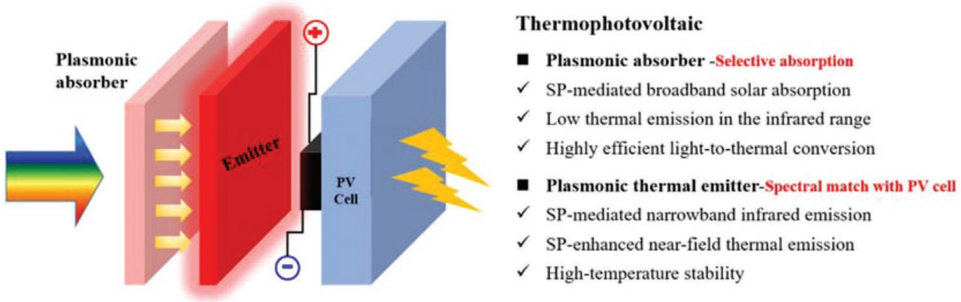

Figure 18. Schematic illustration of TPV and key components with the desired performance.

including cermet-based multilayers,[256,257] MIM configurations,[258,259] and alternating insulator–metal–insulator (IMI) multilayer stacks.[260,261] Notably, the design strategies for light absorption also apply to thermal emission according to Kirchhoff's law,[262] except for the goal toward narrowband IR emission of the latter. In contrast to selective emitters for TPV, an opposite concept involves the design of selective emitters with nearly no absorption (total reflection) across the solar spectrum, but high absorptivity/emissivity within the IR transparency window of the atmosphere (8–13 µm). This gives rise to the revolutionary passive daytime radiative cooling (PDRC) techniques and application prospects in energy-efficient buildings, smart textiles, water harvesting, device cooling, etc.[263] PDRC harvests the coldness of the universe by exploiting the balance of radiative heat flow, thus achieving effective daytime subambient cooling. Various selective emitters with engineered photonic structures such as the polymer-coated fused SiO_2 mirror,[264] hierarchically designed polymer nanofiber-based film,[265] hierarchical-morphology metafabric,[266] etc., have been fabricated, all of which exhibit excellent PDRC performance. For more detailed information, one can refer to literature studies.[263,267]

5.3.1. Multilayer Stacks Based on Plasmonic Cermets

One typical type of selective absorber is based on cermets, i.e., metal–ceramic composite film, in which plasmonic NPs are embedded in a ceramic matrix. They are multilayered stacks with one- or double-layered cermets sandwiched between a bottom IR reflective layer and a top antireflection layer (Figure 18A). In this configuration, the plasmonic NPs in the cermet are mainly responsible for the broadband absorption, due to the excitation of LSPs and the effective coupling between adjacent NPs, together with their intrinsic absorption.[268] Thus, the optical responses of this absorber can be flexibly tailored via manipulating LSP-induced effects of these plasmonic NPs in the cermet layer and also by varying the thickness of both the antireflection and IR reflective layers.[268,269]

A large variety of cermets, consisting of plasmonic metals including Au, Ag, Al, Cu, W, Ta, Mo, etc., as metallic components and ceramic materials such as SiO_2, AlN, Al_2O_3, Si_3N_4, SiC, HfO_2, etc., as the dielectric matrix, has been explored.[270,271] However, noble metals tend to get oxidized or even melt under such a high temperature condition, and nanostructured structures make them more vulnerable due to the size effects. In this case, a dielectric coating may help to address this issue and thus improve the thermal stability. For instance, Au nanostructures coated with a thin layer of alumina have been reported to withstand temperatures of above 800 °C at ambient atmospheric conditions.[272]

For higher-temperature TPV applications, refractory plasmonic materials are more preferred. Metals such as W, Ta, and Mo and transition metal nitrides such as TiN and ZrN are among the most promising candidates (Figure 5C).[64] For example, a solar absorber based on cosputtered W–SiC ultrathin refractory nanocomposite was fabricated,[274] which yielded a full-spectrum solar absorption of 95.45% and a thermal emittance below 5%. The high absorption was ascribed to the coupling of LSPs in the self-formed W nanoclusters, together with the intrinsic absorption of SiC.[274] Very recently, an all-ceramic selective absorber was developed via spontaneous assembly of colloidal TiN NPs into an ultrathin film on a TiN mirror, with

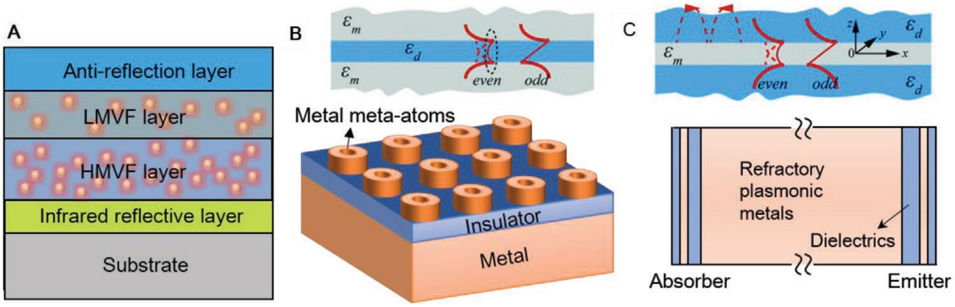

Figure 19. Nanostructured designs for high-temperature TPVs: A) typical selective absorbers of double-cermet-based multilayers; B) plasmonic metamaterial absorbers based on MIM configurations; and C) monolithic planar selective absorber/emitter based on alternating insulator–metal–insulator (IMI) multilayers. Schematic showing SPP modes in (B, C) are redrawn from literature study.[255]

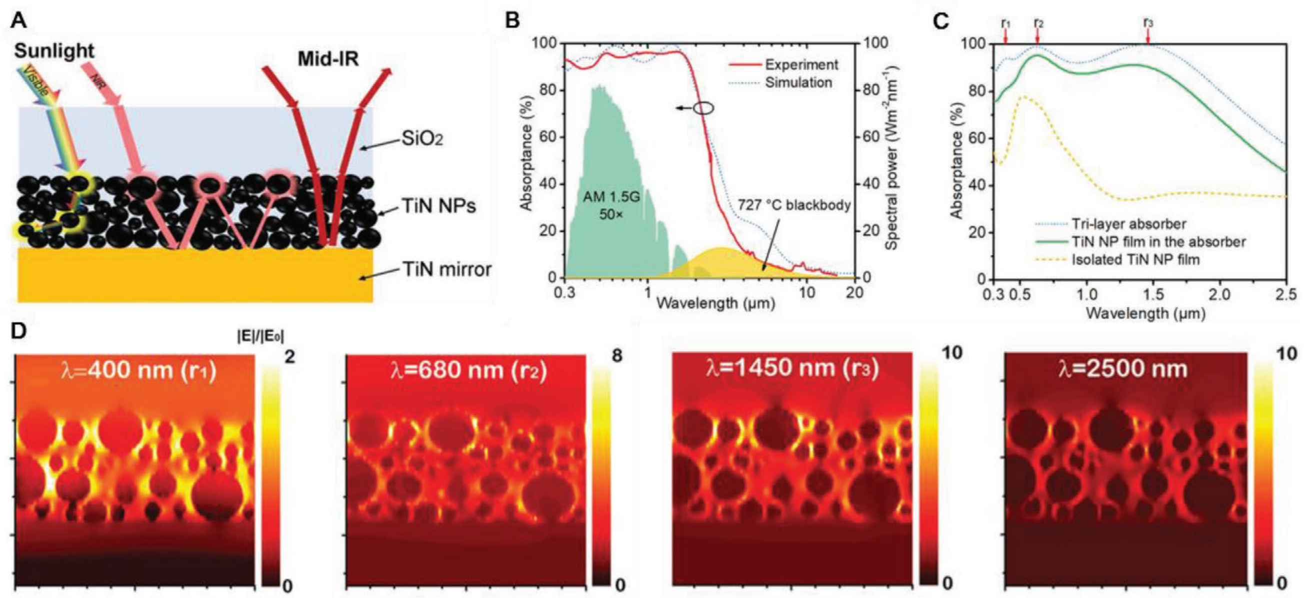

Figure 20. The optical response of the all-ceramic selective absorber and the underlying mechanism: A) schematic showing the nanostructures; B) measured absorption spectrum of the selective absorber compared with the corresponding simulated results; C) comparison of the absorption spectra of the TiN NP film in the trilayer absorber with that of isolated NP film; and D) electric field distributions at different wavelength regions. Reproduced with permission.[273] Copyright 2020, Wiley.

a top SiO_2 antireflection layer (**Figure 20**).[273] It exhibited a full-spectrum near-perfect absorption (95%) and a low thermal emission (3% at 100 °C) at MIR, which was attributed to the synergistic coupling between the in-plane LSPs of NPs and out-of-plane Fabry–Pérot resonance of the NP film and the reflector. Moreover, the proposed absorber exhibited excellent thermal stability and yielded a photothermal efficiency of about 86% under 1000 K.

5.3.2. Metal–Insulator–Metal Metamaterials

MIM configurations have also been widely investigated as TPV absorbers.[141,275–277] As a typical type of plasmonic metamaterial absorbers (PMAs), MIM configurations often consist of a top periodic metallic "meta-atom" layer deposited on a middle insulator layer and a bottom reflective layer. The SPP modes in this MIM configuration with the topmost continuous metal film are schematically displayed in Figure 19B.[255] When the topmost continuous metal film is patterned into periodic "meta-atoms," LSPs in these subwavelength nanostructures as well as strong intra- and intercoupling effects can be flexibly manipulated to achieve the desired performance.[258] Herein, "M" in MIM stands for a more general concept that includes all materials with metallic properties. Tremendous research attempts have been made to explore various combinations of materials and "meta-atom" designs for targeted applications.[259,278,279]

For instance, a refractory plasmonic absorber based on TiN/SiO_2/TiN configuration with the topmost "meta-atom" layer patterned as square rings was fabricated, which yielded an average absorption of 95% from visible to NIR region (**Figure 21**A).[68] This good performance stems from both the intra- and intercoupling of LSPs in and between the symmetric square ring unit cells, together with the intrinsic absorption of TiN. Similarly, a MIM-based integrated absorber/emitter for TPV was designed, which consisted of hexagonally packed W doughnuts (hexarings) placed on AlN/W layers. A broadband solar absorption of over 85% ranging from 0.3 to 2.18 μm and a thermal emission of 100% at 2.18 μm were achieved (Figure 21B).[280] The mechanisms also involve the combination of LSP-mediated absorption enhancement in the near-IR region and the high intrinsic loss of W in the visible region. The hexaring structure induces intraparticle coupling of LSPs due to its hollow feature and more easily tends to achieve perfect impedance matching with air. Moreover, magnetic dipole oscillations also get excited between the topmost patterning layer and the ground W layer to induce zero reflectance and complete absorption.

Many other "meta-atoms" with various structures including gratings,[282,283] crosses,[260,284] pyramids,[141,285] etc., have also been explored to improve the absorption in TPV. Furthermore, hybrid strategies can also be applied for achieving mutual overlapping and coupling of more resonant modes to broaden the absorption spectrum.[149] Figure 21C displays that a PMA has been recently explored via patterning the topmost metal layer into a collection of multiple cubes, cylinders, and cross-resonators with different sizes, thus achieving near-perfect broadband absorption.[281]

5.3.3. Alternating Insulator–Metal–Insulator Multilayer Stacks

IMI structure, with subwavelength layer thickness, is another common configuration for absorbers/emitters used in TPV. The SPPs can be excited at both sides of the middle metal film that are coupled to generate new symmetric and antisymmetric modes (Figure 18C). In this case, the symmetric mode

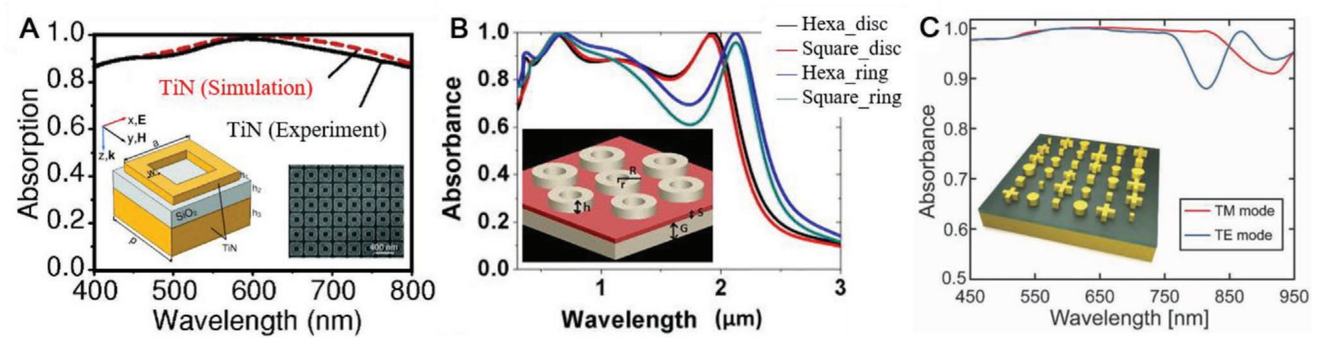

Figure 21. Metamaterial solar absorbers based on MIM configuration. A) Absorption spectrum of the three-layer TiN metamaterial absorber compared with simulated results, with insets illustrating the schematic of the nanostructure and SEM image of the as-fabricated absorber. Reproduced with permission.[68] Copyright 2014, Wiley. B) Comparison of absorption spectra for plasmonic metamaterial absorbers with various top metal unit cells, with insets showing the schematic of the W hexa-doughnut-based nanostructure. Reproduced with permission.[280] Copyright 2017, AIP. C) Simulated absorption spectra for the transverse electric (TE) and transverse magnetic (TM) mode of the proposed MIM superabsorber structure shown in the inset. Reproduced with permission.[281] Copyright 2018, Wiley.

exhibits stronger field localization compared with the antisymmetric mode,[255] thus resulting in higher light absorption and energy concentration within specific spectral ranges. Therefore, the SPP modes can be manipulated by optimizing the thickness of each layer to enable selective absorption/emission. In this configuration, both the selective absorber and emitter are monolithically integrated on a planar substrate made of refractory plasmonic metals (Figure 18C). For instance, a monolithic, planar, and spectrally selective absorber/emitter consisting of thin-film W sandwiched by yttria-stabilized zirconia layers was fabricated. When integrated with a narrow-bandgap (0.67 eV) GaSb cell, the light-to-electricity conversion efficiency of 23% was achieved.[256] A similar design was obtained using Mo and HfO_2 coatings.[257] This simple design can be easily fabricated and it is helpful for the device to remain thermally stable.

The capacity of thermoplasmonics to manipulate light and heat at the nanoscale also offers inspiration to design other configurations for high-temperature TPVs. For instance, photonic crystals based on refractory plasmonic metals as monolithic absorbers/emitters[286,287] and near-field TPV by bringing the emitter and PV cell in the subwavelength distance,[288,289] have been explored. For the latter, materials supporting surface polaritons in the IR ranges, e.g., polar dielectrics such as SiC, SiO_2, etc., and 2D vdW materials such as graphene, hexagonal boron nitride (h-BN), etc., hold great promise as potential candidates to further boost the overall efficiency of near-field TPVs.[290,291] Although significant progress has advanced and a record-high efficiency of up to 29.1% has been demonstrated so far,[292] it is still far below the theoretical capability. Further research efforts are required in terms of reducing parasitic thermal losses in PV cells, which can improve the thermal stability of both materials and devices and aid in the development of innovative PV cells with narrower bandgaps, and so on.

6. Challenges and Future Perspectives

Plasmonic materials and nanostructures with well-designed SPs and thermal responses have shown great potential for diverse applications in the solar energy field. This is attributed to the high energy concentration that allows for miniaturization of solar harvesting devices, the generated hot carriers enabling high efficiency of solar-to-electricity/chemical energy conversions, and the controllable heat generation that derives more diversified utilization.[7] Although great scientific achievements have been made in the past decades, several major challenges still need to be addressed to allow all these technologies to be effectively used in large-scale implementations. Undeniably, ongoing efforts are warranted in terms of both fundamental research and practical explorations to strike a balance among requirements for the overall efficiency, long-term stability, scalability, and cost-effectiveness at every level from materials, nanostructure engineering, to system integration (**Figure 22**).

6.1. Fundamental Research

A complete physical picture for mechanisms involved in thermoplasmonics still remains to be created, such as nonequilibrium plasmonics involving ultrafast dynamics of both hot carriers and thermalization. Comprehensive understanding of the ultrafast dynamics of hot carriers, i.e., their excitation, relaxation, and transfer in materials is the key to extracting or converting them.[124] The latter is closely related to the final lattice thermalization, where the electron–phonon interaction matters. For plasmonic photothermal catalysts, the more efficient and accurate design, such as presence of numerous active sites on single catalysts, often roots in the clearer theoretical insights into the structure–reactivity relationship. The contributions from the thermal and nonthermal mechanisms remain to be disentangled for specific plasmon-driven reactions toward better performance.[73,124,214,216] On the other hand, the LSP-induced heating of NPs has been shown to enable boiling of water in both evaporation and catalytic systems.[188,231] However, the fundamental understanding of energy flux for the phase change at this scale still remains unclear.[7] Besides, the nonlinear thermo-optical effects in thermoplasmonics remain relatively ill-explored. Undeniably, a lot more systematic research efforts on this topic can be beneficial for system optimization in the future plasmonic-based thermal reactors or

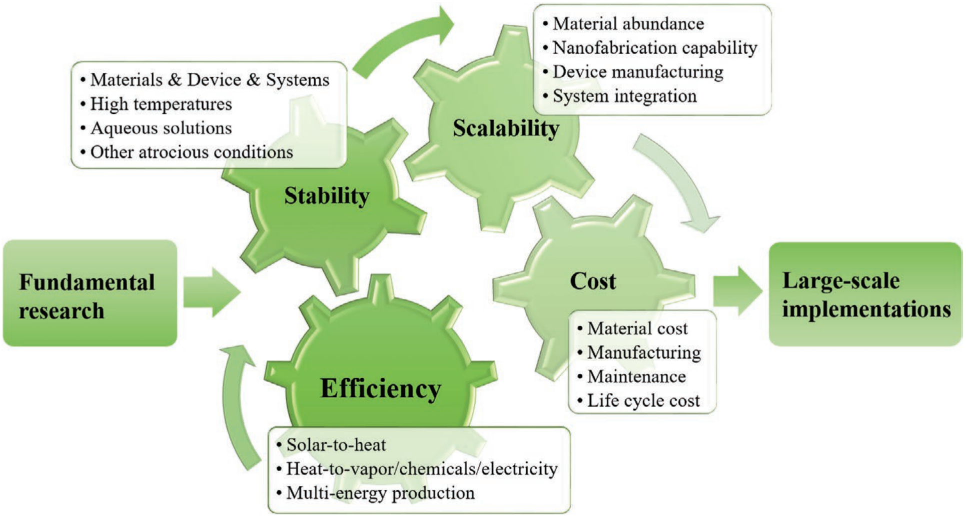

Figure 22. Schematic illustration of overall consideration of the large-scale implementation of the solar-driven thermoplasmonic-based applications.

absorbers/emitters in different temperature regimes. Robust nanothermometry with a spatiotemporal resolution in nanometer–picosecond region remains to be developed and is expected to serve as an indispensable tool to clarify these issues.

This incomplete physical image also challenges the ability of researchers to construct efficient theoretical models capable of describing the diverse phenomena in thermoplasmonics. Classical frameworks of both EM and thermodynamics along with (semi)empirical constitutive parameters including material permittivity, heat capacity, heat conductivity, etc., are no longer eligible because the spatial scale approaches the atomic level.[14,41,118] In this context, ab initio understanding in modeling nonequilibrium plasmonics is necessary and highly desirable to unravel these ultrafast dynamical processes at the atomic scale.300 Besides, multiscale models are further required to explore mutual interactions such as electron–phonon scattering and heat transport between realistic systems. Therefore, a combination of modeling approaches, i.e., the atomistic ab initio methods, molecular dynamics, and semiclassical optical/thermal models will be promising to provide integrated information from atomistic scale to larger-scale systems. This will be particularly important when studying hybrid design strategies with different materials and nanostructures.

6.2. Further Improvement in Efficiency and Long-Term Stability

Despite steady progress, the overall energy conversion efficiency of these solar systems requires further improvements. Nanostructured-mediated thermal management can be systematically explored to further reduce heat losses and thus increase the system efficiency regardless of solar concentration.[197] Deep insights into the coupling of solar absorption, photothermal conversion, heat/mass transport, and many other dynamic processes involved in evaporation/catalysis systems are also beneficial for system optimization. Methods to further increase the efficiency of TPV may lie in either recycling photons via spectral engineering or by exploiting the near-field tunneling effects of thermally stimulated photons. Besides, one development trend of these thermoplasmonic-based solar applications involves the multienergy coproduction in a standalone hybrid system attributed to the involvement of diverse energy conversions. In this way, the system efficiency together with the solar energy utilization ratio can be further increased through cascade utilization of energy. Many innovative concepts, including the concurrent solar desalination and catalytic hydrogen generation,[250,173] simultaneous production of fresh water and electricity,[20,107] integration with thermal energy storage technologies,[293] etc., have been demonstrated.

Long-term stability of currently used devices and systems requires further study to achieve longer lifecycles when exposed to solar irradiation and solution immersion/high temperature conditions. To this end, a better understanding of the degradation mechanisms in nanostructures, such as fouling issues in various solution environments and the diffusion of dielectric grains under high temperatures, is highly desirable.[198,294] At the system level, it would be valuable to test its stability in the long run under transient and real working conditions. Notably, realizing multienergy coproduction in a hybrid system is beneficial, but calls for higher demands on the system stability as more volatile working conditions are often involved.

6.3. Scalability and Cost-Effectiveness toward Large-Scale Implementation

Cost-effectiveness and scalability are the other two key factors for the commercialization of these technologies. Given the currently explored systems, the expenses remain prohibitively high for large-scale installations. First, the material cost remains high especially when noble metallic nanostructures are adopted. Second, the costly nanofabrication processes such as EBL and FIB are often required to realize elaborate nanostructured designs including metasurface, photonic crystals, etc. Third, optical concentrators with the solar-tracking systems are often required to achieve highly concentrated solar irradiation and high temperature, which surges the capital cost. Finally, related land use, system operation, maintenance, etc., may further increase the entire process life-cycle cost. Despite some interfacial evaporation systems have yielded high evaporation efficiencies under one sun via thermal concentration, which resulted in significant reduction in the cost by avoiding the use of optical concentrators.[131,210] More attempts are still required to be made to cut down the cost of materials, improve the nanofabrication, and favor the system integration, and to ensure the scalability of every component and step. For instance, the material cost can be significantly reduced by replacing noble metals with inexpensive materials, such as Al, TiN, etc., or recycling materials via centrifugation or magnetization.[295,296] However, previous and current studies provide very limited information about the cost of the designed materials and/or nanostructures as well as the estimated manufacturing scalability, making it very difficult to evaluate the commercial potential of these technologies. More attentions should be paid on this aspect and further insights will benefit the entire solar energy field.

6.4. Exploration of New Materials and Structural Designs

These three applications have benefited tremendously from various materials and nanostructured designs. However, their large-scale implementations require further material and structural innovation. New materials featuring favorable thermoplasmonic properties together with long-term stability, cost-effectiveness, abundance, easy access and process, etc., should be highly addressed and fundamentally employed. Low-dimensional materials such as graphene, with gate-tunable SPs in the IR range and very high thermal conductivity, offer new channels for heat transport and active thermal control;[297,298] While 2D MXenes, such as $Ti_3C_2T_x$ and a large family of members, have demonstrated intrinsically excellent spectral selectivity and photothermal conversion, which can avoid costly post-nanofabrication process and is quite promising for solar thermal applications.[299] For structural designs, bionics may provide inspiration for revolutionary innovations. Nanofabrication techniques will continue to play a key role in order to realize all these elaborated designs. In this sense, thermoplasmonic-assisted synthesis or fabrication may serve as a powerful tool.

Though further research developments are desired, the intrinsic advantages of thermoplasmonics imply that it can not only optimize the harvesting and conversion of solar energy, but also facilitate clean energy production and emission reduction, thus contributing to the achievement of the national targets toward carbon peak and carbon neutrality.

Acknowledgements

The authors greatly acknowledge the financial support from the National Natural Science Foundation of China (Grant No. 51925203), the Strategic Priority Research Program of Chinese Academy of Sciences (Grant No. XDB36000000), and the Special Research Assistant Program of Chinese Academy of Sciences.

Conflict of Interest

The authors declare no conflict of interest.

Keywords

applications, nanostructured designs, plasmonic materials, solar energy, thermoplasmonics

Received: September 15, 2021
Revised: March 4, 2022

[1] *Net Zero by 2050 - A Roadmap for the Global Energy Sector*, International Energy Agency, Paris 75015, France **2021**, https://iea.blob.core.windows.net/assets/063ae08a-7114-4b58-a34e-39db2112d0a2/NetZeroby2050-ARoadmapfortheGlobalEnergySector.pdf.
[2] C. Hepburn, Y. Qi, N. Stern, B. Ward, C. Xie, D. Zenghelis, *Environ. Sci. Ecotechnol.* **2021**, *8*, 100130.
[3] B. Sorensen, *Renewable Energy: Physics, Engineering, Environmental Impacts, Economics and Planning*, 5th ed., Elsevier, Amsterdam **2017**.
[4] J. Twidell, T. Weir, *Renewable Energy Resources*, Routledge, New York **2015**.
[5] G. N. Tiwari, A. Tiwari, Shyam, *Handbook of Solar Energy*, Springer Nature, Singapore **2016**.
[6] I. Yahyaoui, *Advances in Renewable Energies and Power Technologies: Volume 1: Solar and Wind Energies*, Elsevier Science Ltd, Oxford **2018**.
[7] S. V. Boriskina, H. Ghasemi, G. Chen, *Mater. Today* **2013**, *16*, 375.
[8] J. A. Schuller, E. S. Barnard, W. Cai, Y. C. Jun, J. S. White, M. L. Brongersma, *Nat. Mater.* **2010**, *9*, 193.
[9] G. BAFFOU, *Thermoplasmonics: Heating Metal Nanoparticles Using Light*, Cambridge University Press, Cambridge **2018**.
[10] G. Baffou, R. Quidant, *Laser Photonics Rev.* **2013**, *7*, 171.
[11] M. Mutlu, J. H. Kang, S. Raza, D. Schoen, X. Zheng, P. G. Kik, M. L. Brongersma, *Nano Lett.* **2018**, *18*, 1699.
[12] A. R. Rastinehad, H. Anastos, E. Wajswol, J. S. Winoker, J. P. Sfakianos, S. K. Doppalapudi, M. R. Carrick, C. J. Knauer, B. Taouli, S. C. Lewis, A. K. Tewari, J. A. Schwartz, S. E. Canfield, A. K. George, J. L. West, N. J. Halas, *Proc. Natl. Acad. Sci. USA* **2019**, *116*, 18590.
[13] V. P. Pattani, J. W. Tunnell, *Lasers Surg. Med.* **2012**, *44*, 675.
[14] M. Zhu, G. Baffou, N. Meyerbröker, J. Polleux, *ACS Nano* **2012**, *6*, 7227.
[15] B. C. Stipe, T. C. Strand, C. C. Poon, H. Balamane, T. D. Boone, J. A. Katine, J. L. Li, V. Rawat, H. Nemoto, A. Hirotsune, O. Hellwig, R. Ruiz, E. Dobisz, D. S. Kercher, N. Robertson, T. R. Albrecht, B. D. Terris, *Nat. Photonics* **2010**, *4*, 484.
[16] A. Furube, S. Hashimoto, *NPG Asia Mater.* **2017**, *9*, e454.
[17] S. Hashimoto, D. Werner, T. Uwada, *J. Photochem. Photobiol., C* **2012**, *13*, 28.
[18] L. Mascaretti, A. Naldoni, *J. Appl. Phys.* **2020**, *128*, 041101.
[19] O. A. Balitskii, *Mater. Today Energy* **2021**, *20*, 100629.
[20] M. Gao, L. Zhu, C. K. Peh, G. W. Ho, *Energy Environ. Sci.* **2019**, *12*, 841.
[21] G. Baffou, F. Cichos, R. Quidant, *Nat. Mater.* **2020**, *19*, 946.
[22] A. Naldoni, V. M. Shalaev, M. L. Brongersma, *Science* **2017**, *356*, 908.
[23] M. I. Stockman, K. Kneipp, S. I. Bozhevolnyi, S. Saha, A. Dutta, J. Ndukaife, N. Kinsey, H. Reddy, U. Guler, V. M. Shalaev, A. Boltasseva, B. Gholipour, H. N. S. Krishnamoorthy, K. F. MacDonald, C. Soci, N. I. Zheludev, V. Savinov, R. Singh, P. Groß, C. Lienau, M. Vadai, M. L. Solomon, D. R. Barton, M. Lawrence, J. A. Dionne, S. V. Boriskina, R. Esteban, J. Aizpurua, X. Zhang, S. Yang, et al., *J. Opt.* **2018**, *20*, 043001.
[24] S. A. Maier, *Plasmonics: Fundamentals and Applications*, Springer, Berlin **2007**.

[25] A. Agrawal, S. H. Cho, O. Zandi, S. Ghosh, R. W. Johns, D. J. Milliron, *Chem. Rev.* **2018**, *118*, 3121.
[26] S. V. Boriskina, T. Cooper, L. Zeng, G. Ni, J. K. Tong, Y. Tsurimaki, Y. Huang, L. Meroueh, G. Mahan, G. Chen, *Adv. Opt. Photonics* **2018**, *9*, 775.
[27] M. L. Brongersma, N. J. Halas, P. Nordlander, *Nat. Nanotechnol.* **2015**, *10*, 25.
[28] J. G. Liu, H. Zhang, S. Link, P. Nordlander, *ACS Photonics* **2018**, *5*, 2584.
[29] M. Bernardi, J. Mustafa, J. B. Neaton, S. G. Louie, *Nat. Commun.* **2015**, *6*, 7044.
[30] B. Y. Zheng, H. Zhao, A. Manjavacas, M. McClain, P. Nordlander, N. J. Halas, *Nat. Commun.* **2015**, *6*, 7797.
[31] G. Baffou, P. Berto, E. Bermúdez Ureña, R. Quidant, S. Monneret, J. Polleux, H. Rigneault, *ACS Nano* **2013**, *7*, 6478.
[32] L. Jauffred, A. Samadi, H. Klingberg, P. M. Bendix, L. B. Oddershede, *Chem. Rev.* **2019**, *119*, 8087.
[33] P. R. West, S. Ishii, G. V. Naik, N. K. Emani, V. M. Shalaev, A. Boltasseva, *Laser & Photonics Reviews* **2010**, *4*, 795.
[34] G. V. Naik, V. M. Shalaev, A. Boltasseva, *Adv. Mater.* **2013**, *25*, 3264.
[35] B. Craig F, H. Donald R, *Absorption and Scattering of Light by Small Particles*, Wiley-VCH, Weinheim **1983**.
[36] J. Cunha, T.-L. Guo, A. N. Koya, A. Toma, M. Prato, G. Della Valle, A. Alabastri, R. P. Zaccaria, *Adv. Opt. Mater.* **2020**, *8*, 2000568.
[37] Y. Huang, Y.-H. Pan, R. Yang, L.-H. Bao, L. Meng, H.-L. Luo, Y.-Q. Cai, G.-D. Liu, W.-J. Zhao, Z. Zhou, L.-M. Wu, Z.-L. Zhu, M. Huang, L.-W. Liu, L. Liu, P. Cheng, K.-H. Wu, S.-B. Tian, C.-Z. Gu, Y.-G. Shi, Y.-F. Guo, Z. G. Cheng, J.-P. Hu, L. Zhao, G.-H. Yang, E. Sutter, P. Sutter, Y.-L. Wang, W. Ji, X.-J. Zhou, et al., *Nat. Commun.* **2020**, *11*, 2453.
[38] H. H. Richardson, M. T. Carlson, P. J. Tandler, P. Hernandez, A. O. Govorov, *Nano Lett.* **2009**, *9*, 1139.
[39] R. W. Schoenlein, W. Z. Lin, J. G. Fujimoto, G. L. Eesley, *Phys. Rev. Lett.* **1987**, *58*, 1680.
[40] A. Block, M. Liebel, R. Yu, M. Spector, Y. Sivan, F. J. García de Abajo, N. F. van Hulst, *Sci. Adv.* **2019**, *5*, eaav8965.
[41] X. Hou, N. Djellali, B. Palpant, *ACS Photonics* **2018**, *5*, 3856.
[42] A. Schirato, M. Maiuri, A. Toma, S. Fugattini, R. Proietti Zaccaria, P. Laporta, P. Nordlander, G. Cerullo, A. Alabastri, G. Della Valle, *Nat. Photonics* **2020**, *14*, 723.
[43] A. Alabastri, A. Toma, M. Malerba, F. De Angelis, R. P. Zaccaria, *ACS Photonics* **2015**, *2*, 115.
[44] M. Ferrera, M. Magnozzi, F. Bisio, M. Canepa, *Phys. Rev. Mater.* **2019**, *3*, 105201.
[45] Y. Sivan, S. W. Chu, *Nanophotonics* **2017**, *6*, 317.
[46] A. Alabastri, M. Malerba, E. Calandrini, A. Manjavacas, F. De Angelis, A. Toma, R. P. Zaccaria, *Nano Lett.* **2017**, *17*, 5472.
[47] R. J. Mendelsberg, G. Garcia, D. J. Milliron, *J. Appl. Phys.* **2012**, *111*, 063515.
[48] A. Boltasseva, H. A. Atwater, *Science* **2011**, *331*, 290.
[49] J. B. Khurgin, A. Boltasseva, *MRS Bull.* **2012**, *37*, 768.
[50] A. Lalisse, G. Tessier, J. Plain, G. Baffou, *J. Phys. Chem. C* **2015**, *119*, 25518.
[51] H. Chen, L. Shao, Q. Li, J. Wang, *Chem. Soc. Rev.* **2013**, *42*, 2679.
[52] H. Kang, J. T. Buchman, R. S. Rodriguez, H. L. Ring, J. He, K. C. Bantz, C. L. Haynes, *Chem. Rev.* **2019**, *119*, 664.
[53] Y. A. Krutyakov, A. A. Kudrinskiy, A. Y. Olenin, G. V Lisichkin, *Russ. Chem. Rev.* **2008**, *77*, 233.
[54] A. Marimuthu, J. Zhang, S. Linic, *Science* **2013**, *340*, 1590.
[55] B. D. Clark, C. R. Jacobson, M. Lou, J. Yang, L. Zhou, S. Gottheim, C. J. DeSantis, P. Nordlander, N. J. Halas, *Nano Lett.* **2018**, *18*, 1234.
[56] X. Zhu, G. M. Imran Hossain, M. George, A. Farhang, A. Cicek, A. A. Yanik, *ACS Photonics* **2020**, *7*, 416.
[57] S. Tian, O. Neumann, M. J. McClain, X. Yang, L. Zhou, C. Zhang, P. Nordlander, N. J. Halas, *Nano Lett.* **2017**, *17*, 5071.
[58] C. R. Jacobson, D. Solti, D. Renard, L. Yuan, M. Lou, N. J. Halas, *Acc. Chem. Res.* **2020**, *53*, 2020.
[59] B. D. Clark, C. R. Jacobson, M. Lou, D. Renard, G. Wu, L. Bursi, A. S. Ali, D. F. Swearer, A. L. Tsai, P. Nordlander, N. J. Halas, *ACS Nano* **2019**, *13*, 9682.
[60] H. Robatjazi, D. Weinberg, D. F. Swearer, C. Jacobson, M. Zhang, S. Tian, L. Zhou, P. Nordlander, N. J. Halas, *Sci. Adv.* **2019**, *5*, eaav5340.
[61] B. D. Clark, M. Lou, P. Nordlander, N. J. Halas, *Nano Lett.* **2020**, *20*, 6644.
[62] A. Sobhani, A. Manjavacas, Y. Cao, M. J. McClain, F. J. García de Abajo, P. Nordlander, N. J. Halas, *Nano Lett.* **2015**, *15*, 6946.
[63] M. B. Ross, G. C. Schatz, *J. Phys. D: Appl. Phys.* **2015**, *48*, 184004.
[64] U. Guler, A. Boltasseva, V. M. Shalaev, *Science* **2014**, *344*, 263.
[65] G. V. Naik, *Alternative Plasmonic Materials*, Elsevier Ltd, Amsterdam **2018**.
[66] J. M. Luther, P. K. Jain, T. Ewers, A. P. Alivisatos, *Nat. Mater.* **2011**, *10*, 361.
[67] S. W. Verbruggen, M. Keulemans, J. A. Martens, S. Lenaerts, *J. Phys. Chem. C* **2013**, *117*, 19142.
[68] W. Li, U. Guler, N. Kinsey, G. V. Naik, A. Boltasseva, J. Guan, V. M. Shalaev, A. V. Kildishev, *Adv. Mater.* **2014**, *26*, 7959.
[69] U. Guler, V. M. Shalaev, A. Boltasseva, *Mater. Today* **2015**, *18*, 227.
[70] S. Ishii, R. P. Sugavaneshwar, T. Nagao, *J. Phys. Chem. C* **2016**, *120*, 2343.
[71] L. Wang, G. Zhu, M. Wang, W. Yu, J. Zeng, X. Yu, H. Xie, Q. Li, *Sol. Energy* **2019**, *184*, 240.
[72] D. Jiang, W. Yang, *Sol. Energy Mater. Sol. Cells* **2017**, *163*, 98.
[73] S. Rej, L. Mascaretti, E. Y. Santiago, O. Tomanec, Š. Kment, Z. Wang, R. Zbořil, P. Fornasiero, A. O. Govorov, A. Naldoni, *ACS Catal.* **2020**, *10*, 5261.
[74] J. Ren, A. Zhang, X. Wang, *Mater. Today Energy* **2020**, *100629*, 104743.
[75] H. Salihoglu, W. Nam, L. Traverso, M. Segovia, P. K. Venuthurumilli, W. Liu, Y. Wei, W. Li, X. Xu, *Nano Lett.* **2020**, *20*, 6091.
[76] A. Comin, L. Manna, *Chem. Soc. Rev.* **2014**, *43*, 3957.
[77] S. D. Lounis, E. L. Runnerstrom, A. Llordés, D. J. Milliron, *J. Phys. Chem. Lett.* **2014**, *5*, 1564.
[78] T. M. Mattox, X. Ye, K. Manthiram, P. J. Schuck, A. P. Alivisatos, J. J. Urban, *Adv. Mater.* **2015**, *27*, 5830.
[79] G. Gabka, P. Bujak, A. Ostrowski, W. Tomaszewski, W. Lisowski, J. W. Sobczak, A. Pron, *Inorg. Chem.* **2016**, *55*, 6660.
[80] M. Gong, D. Ewing, M. Casper, A. Stramel, A. Elliot, J. Z. Wu, *ACS Appl. Mater. Interfaces* **2019**, *11*, 19286.
[81] Q. Liu, Y. Wu, J. Zhang, K. Chen, C. Huang, H. Chen, X. Qiu, *Appl. Surf. Sci.* **2019**, *490*, 395.
[82] K. Manthiram, A. P. Alivisatos, *J. Am. Chem. Soc.* **2012**, *134*, 3995.
[83] W. Xu, H. Liu, D. Zhou, X. Chen, N. Ding, H. Song, H. Ågren, *Nano Today* **2020**, *33*, 100892.
[84] K. Hantanasirisakul, Y. Gogotsi, *Adv. Mater.* **2018**, *30*, 1804779.
[85] G. R. Bhimanapati, Z. Lin, V. Meunier, Y. Jung, J. Cha, S. Das, D. Xiao, Y. Son, M. S. Strano, V. R. Cooper, L. Liang, S. G. Louie, E. Ringe, W. Zhou, S. S. Kim, R. R. Naik, B. G. Sumpter, H. Terrones, F. Xia, Y. Wang, J. Zhu, D. Akinwande, N. Alem, J. A. Schuller, R. E. Schaak, M. Terrones, J. A. Robinson, *ACS Nano* **2015**, *9*, 11509.
[86] A. N. Grigorenko, M. Polini, K. S. Novoselov, *Nat. Photonics* **2012**, *6*, 749.
[87] H. Zhang, B. Abhiraman, Q. Zhang, J. Miao, K. Jo, S. Roccasecca, M. W. Knight, A. R. Davoyan, D. Jariwala, *Nat. Commun.* **2020**, *11*, 3552.

[88] T. Low, R. Roldán, H. Wang, F. Xia, P. Avouris, L. M. Moreno, F. Guinea, *Phys. Rev. Lett.* **2014**, *113*, 5.
[89] D. N. Basov, M. M. Fogler, F. J. García de Abajo, *Science* **2016**, *354*, aag1992.
[90] T. Low, A. Chaves, J. D. Caldwell, A. Kumar, N. X. Fang, P. Avouris, T. F. Heinz, F. Guinea, L. Martin-Moreno, F. Koppens, *Nat. Mater.* **2017**, *16*, 182.
[91] Y. Wang, J. Z. Ou, A. F. Chrimes, B. J. Carey, T. Daeneke, M. M. Y. A. Alsaif, M. Mortazavi, S. Zhuiykov, N. Medhekar, M. Bhaskaran, J. R. Friend, M. S. Strano, K. Kalantar-Zadeh, *Nano Lett.* **2015**, *15*, 883.
[92] B. Anasori, M. R. Lukatskaya, Y. Gogotsi, *Nat. Rev. Mater.* **2017**, *2*, 16098.
[93] J. Pang, R. G. Mendes, A. Bachmatiuk, L. Zhao, H. Q. Ta, T. Gemming, H. Liu, Z. Liu, M. H. Rummeli, *Chem. Soc. Rev.* **2019**, *48*, 72.
[94] A. D. Dillon, M. J. Ghidiu, A. L. Krick, J. Griggs, S. J. May, Y. Gogotsi, M. W. Barsoum, A. T. Fafarman, *Adv. Funct. Mater.* **2016**, *26*, 4162.
[95] A. VahidMohammadi, J. Rosen, Y. Gogotsi, *Science* **2021**, *372*, eabf1581.
[96] H. Lin, X. Wang, L. Yu, Y. Chen, J. Shi, *Nano Lett.* **2017**, *17*, 384.
[97] K. Chaudhuri, M. Alhabeb, Z. Wang, V. M. Shalaev, Y. Gogotsi, A. Boltasseva, *ACS Photonics* **2018**, *5*, 1115.
[98] R. Li, L. Zhang, L. Shi, P. Wang, *ACS Nano* **2017**, *11*, 3752.
[99] D. Xu, Z. Li, L. Li, J. Wang, *Adv. Funct. Mater.* **2020**, *30*, 2000712.
[100] C. Mouhot, C. Villani, *Acta Math.* **2011**, *207*, 29.
[101] E. Ringe, M. R. Langille, K. Sohn, J. Zhang, J. Huang, C. A. Mirkin, R. P. Van Duyne, L. D. Marks, *J. Phys. Chem. Lett.* **2012**, *3*, 1479.
[102] G. Baffou, R. Quidant, C. Girard, *Appl. Phys. Lett.* **2009**, *94*, 153109.
[103] X. Lu, M. Rycenga, S. E. Skrabalak, B. Wiley, Y. Xia, *Annu. Rev. Phys. Chem.* **2009**, *60*, 167.
[104] J. B. Lassiter, M. W. Knight, N. A. Mirin, N. J. Halas, *Nano Lett.* **2009**, *9*, 4326.
[105] E. Prodan, C. Radloff, N. J. Halas, P. Nordlander, *Science* **2003**, *302*, 419.
[106] L. Wang, Y. Wang, P. Schmuki, S. Kment, R. Zboril, *Electrochim. Acta* **2018**, *260*, 212.
[107] M. Gao, C. K. Peh, H. T. Phan, L. Zhu, G. W. Ho, *Adv. Energy Mater.* **2018**, *8*, 1800711.
[108] R. González-Campuzano, J. M. Saniger, D. Mendoza, *Nanotechnology* **2017**, *28*, 465704.
[109] J. A. Webb, W. R. Erwin, H. F. Zarick, J. Aufrecht, H. W. Manning, M. J. Lang, C. L. Pint, R. Bardhan, *J. Phys. Chem. C* **2014**, *118*, 3696.
[110] H. Wang, Y. Wu, B. Lassiter, C. L. Nehl, J. H. Hafner, P. Nordlander, M. J. Halas, *Proc. Natl. Acad. Sci. USA* **2006**, *103*, 10856.
[111] A. M. Goodman, Y. Cao, C. Urban, O. Neumann, C. Ayala-Orozco, M. W. Knight, A. Joshi, P. Nordlander, N. J. Halas, *ACS Nano* **2014**, *8*, 3222.
[112] M. Prieto, R. Arenal, L. Henrard, L. Gomez, V. Sebastian, M. Arruebo, *J. Phys. Chem. C* **2014**, *118*, 28804.
[113] C. Charnay, A. Lee, S. Q. Man, C. E. Moran, C. Radloff, R. K. Bradley, N. J. Halas, *J. Phys. Chem. B* **2003**, *107*, 7327.
[114] W. Zhang, L. Wang, K. Wang, M. U. Khan, M. Wang, H. Li, J. Zeng, *Small* **2017**, *13*, 1602583.
[115] G. Baffou, R. Quidant, F. J. García de Abajo, *ACS Nano* **2010**, *4*, 709.
[116] B. Gerislioglu, L. Dong, A. Ahmadivand, H. Hu, P. Nordlander, N. J. Halas, *Nano Lett.* **2020**, *20*, 2087.
[117] M. Hentschel, M. Saliba, R. Vogelgesang, H. Giessen, A. P. Alivisatos, N. Liu, *Nano Lett.* **2010**, *10*, 2721.
[118] N. Liu, S. Mukherjee, K. Bao, Y. Li, L. V. Brown, P. Nordlander, N. J. Halas, *ACS Nano* **2012**, *6*, 5482.
[119] X. Wang, H. Li, X. Yu, X. Shi, J. Liu, *Appl. Phys. Lett.* **2012**, *101*, 203109.
[120] P. Huang, J. Lin, W. Li, P. Rong, Z. Wang, S. Wang, X. Wang, X. Sun, M. Aronova, G. Niu, R. D. Leapman, Z. Nie, X. Chen, *Angew. Chem., Int. Ed.* **2013**, *52*, 13958.
[121] B. Lamprecht, G. Schider, R. T. Lechner, H. Ditlbacher, J. R. Krenn, A. Leitner, F. R. Aussenegg, *Phys. Rev. Lett.* **2000**, *84*, 4721.
[122] W. Wang, M. Ramezani, A. I. Väkeväinen, P. Törmä, J. G. Rivas, T. W. Odom, *Mater. Today* **2018**, *21*, 303.
[123] S. Zhang, K. Bao, N. J. Halas, H. Xu, P. Nordlander, *Nano Lett.* **2011**, *11*, 1657.
[124] E. Cortés, L. V Besteiro, A. Alabastri, A. Baldi, G. Tagliabue, A. Demetriadou, P. Narang, *ACS Nano* **2020**, *14*, 16202.
[125] G. Baffou, R. Quidant, C. Girard, *Phys. Rev. B: Condens. Matter Mater. Phys.* **2010**, *82*, 165424.
[126] M. W. Knight, Y. Wu, J. B. Lassiter, P. Nordlander, N. J. Halas, *Nano Lett.* **2009**, *9*, 2188.
[127] H. T. Chorsi, Y. Lee, A. Alù, J. X. J. Zhang, *Sci. Rep.* **2017**, *7*, 15985.
[128] L. Zhou, Y. Tan, J. Wang, W. Xu, Y. Yuan, W. Cai, S. Zhu, J. Zhu, *Nat. Photonics* **2016**, *10*, 393.
[129] L. Zhou, Y. Tan, D. Ji, B. Zhu, P. Zhang, J. Xu, Q. Gan, Z. Yu, J. Zhu, *Sci. Adv.* **2016**, *2*, e1501227.
[130] K. Setoura, Y. Okada, D. Werner, S. Hashimoto, *ACS Nano* **2013**, *7*, 7874.
[131] G. Ni, G. Li, S. V. Boriskina, H. Li, W. Yang, T. J. Zhang, G. Chen, *Nat. Energy* **2016**, *1*, 16126.
[132] S. V. Boriskina, J. K. Tong, W.-C. Hsu, L. Weinstein, X. Huang, J. Loomis, Y. Xu, G. Chen, *Act. Photonic Mater. VII* **2015**, *9546*, 95461U.
[133] M. Chen, Y. He, J. Zhu, D. R. Kim, *Energy Convers. Manage.* **2016**, *112*, 21.
[134] I. Zorić, M. Zäch, B. Kasemo, C. Langhammer, *ACS Nano* **2011**, *5*, 2535.
[135] H. Duan, Y. Zheng, C. Xu, Y. Shang, F. Ding, *Appl. Therm. Eng.* **2019**, *161*, 114192.
[136] G. Zhu, L. Wang, N. Bing, H. Xie, W. Yu, *Energy* **2019**, *183*, 747.
[137] O. Z. Sharaf, N. Rizk, C. P. Joshi, M. Abi Jaoudé, A. N. Al-Khateeb, D. C. Kyritsis, E. Abu-Nada, M. N. Martin, *Energy Convers. Manage.* **2019**, *199*, 112010.
[138] J. Chen, J. Feng, Z. Li, P. Xu, X. Wang, W. Yin, M. Wang, X. Ge, Y. Yin, *Nano Lett.* **2019**, *19*, 400.
[139] C. Chen, L. Zhou, J. Yu, Y. Wang, S. Nie, S. Zhu, J. Zhu, *Nano Energy* **2018**, *51*, 451.
[140] V. S. Wenshan Cai, *Optical Metamaterials: Fundamentals and Applications*, Springer-Verlag, New York **2010**.
[141] G. Liu, X. Liu, J. Chen, Y. Li, L. Shi, G. Fu, Z. Liu, *Sol. Energy Mater. Sol. Cells* **2019**, *190*, 20.
[142] Z. Liu, G. Liu, Z. Huang, X. Liu, G. Fu, *Sol. Energy Mater. Sol. Cells* **2018**, *179*, 346.
[143] Y. Tian, X. Liu, F. Chen, Y. Zheng, *OSA Continuum* **2019**, *2*, 3223.
[144] Z. Wang, T. S. Luk, Y. Tan, D. Ji, M. Zhou, Q. Gan, Z. Yu, *Appl. Phys. Lett.* **2015**, *106*, 101104.
[145] M. Chirumamilla, G. V. Krishnamurthy, K. Knopp, T. Krekeler, M. Graf, D. Jalas, M. Ritter, M. Störmer, A. Y. Petrov, M. Eich, *Sci. Rep.* **2019**, *9*, 7241.
[146] M. Garín, D. Hernández, T. Trifonov, R. Alcubilla, *Sol. Energy Mater. Sol. Cells* **2015**, *134*, 22.
[147] V. Tomer, R. Teye-Mensah, J. C. Tokash, N. Stojilovic, W. Kataphinan, E. A. Evans, G. G. Chase, R. D. Ramsier, D. J. Smith, D. H. Reneker, *Sol. Energy Mater. Sol. Cells* **2005**, *85*, 477.
[148] H.-J. Lee, K. Smyth, S. Bathurst, J. Chou, M. Ghebrebrhan, J. Joannopoulos, N. Saka, S.-G. Kim, *Appl. Phys. Lett.* **2013**, *102*, 241904.
[149] L. Feng, P. Huo, Y. Liang, T. Xu, *Adv. Mater.* **2020**, *32*, 1903787.
[150] A. Moreau, C. Ciracì, J. J. Mock, D. R. Smith, R. T. Hill, A. Chilkoti, Q. Wang, B. J. Wiley, *Nature* **2012**, *492*, 86.
[151] Q. Yang, X. Chen, Y. Li, X. Zhang, Y. Xu, Z. Tian, C. Ouyang, J. Gu, J. Han, W. Zhang, *APL Mater.* **2017**, *5*, 096107.
[152] G. Silva-Oelker, C. Jerez-Hanckes, P. Fay, *Opt. Express* **2018**, *26*, A929.

[153] S. Han, J. H. Shin, P. H. Jung, H. Lee, B. J. Lee, *Adv. Opt. Mater.* **2016**, *4*, 1265.
[154] V. Rinnerbauer, S. Ndao, Y. X. Yeng, W. R. Chan, J. J. Senkevich, J. D. Joannopoulos, M. Soljačić, I. Celanovic, *Energy Environ. Sci.* **2012**, *5*, 8815.
[155] Y. Nam, Y. X. Yeng, A. Lenert, P. Bermel, I. Celanovic, M. Soljačić, E. N. Wang, *Sol. Energy Mater. Sol. Cells* **2014**, *122*, 287.
[156] K.-T. Lin, H. Lin, T. Yang, B. Jia, *Nat. Commun.* **2020**, *11*, 1389.
[157] M. Kaur, S. Ishii, S. L. Shinde, T. Nagao, *Adv. Sustainable Syst.* **2019**, *3*, 1800112.
[158] I. E. Khodasevych, L. Wang, A. Mitchell, G. Rosengarten, *Adv. Opt. Mater.* **2015**, *3*, 852.
[159] F. Cao, D. Kraemer, L. Tang, Y. Li, A. P. Litvinchuk, J. Bao, G. Chen, Z. Ren, *Energy Environ. Sci.* **2015**, *8*, 3040.
[160] K. Te Lin, H. L. Chen, Y. S. Lai, C. C. Yu, Y. C. Lee, P. Y. Su, Y. T. Yen, B. Y. Chen, *Nano Energy* **2017**, *37*, 61.
[161] M. Quintanilla, L. M. Liz-Marzán, *Nano Today* **2018**, *19*, 126.
[162] K. Kim, W. Jeong, W. Lee, P. Reddy, *ACS Nano* **2012**, *6*, 4248.
[163] B. Desiatov, I. Goykhman, U. Levy, *Nano Lett.* **2014**, *14*, 648.
[164] Q. Weng, K. T. Lin, K. Yoshida, H. Nema, S. Komiyama, S. Kim, K. Hirakawa, Y. Kajihara, *Nano Lett.* **2018**, *18*, 4220.
[165] J. Zhou, B. del Rosal, D. Jaque, S. Uchiyama, D. Jin, *Nat. Methods* **2020**, *17*, 967.
[166] C. D. S. Brites, P. P. Lima, N. J. O. Silva, A. Millán, V. S. Amaral, F. Palacio, L. D. Carlos, *Nanoscale* **2012**, *4*, 4799.
[167] D. Jaque, F. Vetrone, *Nanoscale* **2012**, *4*, 4301.
[168] M. Runowski, P. Wozny, N. Stopikowska, I. R. Martín, V. Lavín, S. Lis, *ACS Appl. Mater. Interfaces* **2020**, *12*, 43933.
[169] G. Gao, D. Busko, S. Kauffmann-Weiss, A. Turshatov, I. A. Howard, B. S. Richards, *J. Mater. Chem. C* **2018**, *6*, 4163.
[170] D. Wang, Y. R. Koh, Z. A. Kudyshev, K. Maize, A. V. Kildishev, A. Boltasseva, V. M. Shalaev, A. Shakouri, *Nano Lett.* **2019**, *19*, 3796.
[171] S. Linic, P. Christopher, D. B. Ingram, *Nat. Mater.* **2011**, *10*, 911.
[172] M. Elimelech, W. A. Phillip, *Science* **2011**, *333*, 712.
[173] M. Gao, P. K. N. Connor, G. W. Ho, *Energy Environ. Sci.* **2016**, *9*, 3151.
[174] Y. Yen, C. Chen, M. Fang, Y. Chen, C. Lai, C. Hsu, Y. Wang, H. Lin, C. Shen, J. Shieh, J. C. Ho, *Nano Energy* **2015**, *15*, 470.
[175] P. Qiao, J. Wu, H. Li, Y. Xu, L. Ren, K. Lin, W. Zhou, *ACS Appl. Mater. Interfaces* **2019**, *11*, 7066.
[176] X. Li, R. Lin, G. Ni, N. Xu, X. Hu, B. Zhu, G. Lv, J. Li, S. Zhu, J. Zhu, *Natl. Sci. Rev.* **2018**, *5*, 70.
[177] T. Ma, S. Sun, G. Fu, J. W. Hall, Y. Ni, L. He, J. Yi, N. Zhao, Y. Du, T. Pei, W. Cheng, C. Song, C. Fang, C. Zhou, *Nat. Commun.* **2020**, *11*, 650.
[178] L. Rosa, D. D. Chiarelli, M. C. Rulli, J. Dell'Angelo, P. D'Odorico, *Sci. Adv.* **2020**, *6*, eaaz6031.
[179] P. D. Dongare, A. Alabastri, S. Pedersen, K. R. Zodrow, N. J. Hogan, O. Neumann, J. Wud, T. Wang, A. Deshmukh, M. Elimelech, Q. Li, P. Nordlander, N. J. Halas, *Proc. Natl. Acad. Sci. USA* **2017**, *114*, 6936.
[180] Y. Ito, Y. Tanabe, J. Han, T. Fujita, K. Tanigaki, M. Chen, *Adv. Mater.* **2015**, *27*, 4302.
[181] X. Hu, W. Xu, L. Zhou, Y. Tan, Y. Wang, S. Zhu, J. Zhu, *Adv. Mater.* **2017**, *29*, 1604031.
[182] X. Liu, Y. Xuan, *Nanoscale* **2017**, *9*, 14854.
[183] M. S. Zielinski, J. W. Choi, T. La Grange, M. Modestino, S. M. H. Hashemi, Y. Pu, S. Birkhold, J. A. Hubbell, D. Psaltis, *Nano Lett.* **2016**, *16*, 2159.
[184] D. Wang, Y. Fang, W. Yu, L. Wang, H. Xie, Y. Yue, *Sol. Energy Mater. Sol. Cells* **2021**, *220*, 110850.
[185] M. Chen, Y. He, J. Huang, J. Zhu, *Energy Convers. Manage.* **2016**, *127*, 293.
[186] N. J. Hogan, A. S. Urban, C. Ayala-Orozco, A. Pimpinelli, P. Nordlander, N. J. Halas, *Nano Lett.* **2014**, *14*, 4640.
[187] G. Ni, N. Miljkovic, H. Ghasemi, X. Huang, S. V. Boriskina, C. Te Lin, J. Wang, Y. Xu, M. M. Rahman, T. J. Zhang, G. Chen, *Nano Energy* **2015**, *17*, 290.
[188] O. Neumann, A. S. Urban, J. Day, S. Lal, P. Nordlander, N. J. Halas, *ACS Nano* **2013**, *7*, 42.
[189] Z. Fang, Y. R. Zhen, O. Neumann, A. Polman, F. J. García de Abajo, P. Nordlander, N. J. Halas, *Nano Lett.* **2013**, *13*, 1736.
[190] S. Baral, A. J. Green, M. Y. Livshits, A. O. Govorov, H. H. Richardson, *ACS Nano* **2014**, *8*, 1439.
[191] P. Behnam, M. B. Shafii, *Desalination* **2016**, *397*, 30.
[192] M. Taseidifar, M. Shahid, R. M. Pashley, *Desalination* **2018**, *432*, 97.
[193] G. Yao, J. Xu, G. Liu, *Sol. Energy Mater. Sol. Cells* **2020**, *206*, 110292.
[194] Z. Huang, S. Li, X. Cui, Y. Wan, Y. Xiao, S. Tian, H. Wang, X. Li, Q. Zhao, C. S. Lee, *J. Mater. Chem. A* **2020**, *8*, 10742.
[195] S. Chen, Z. Sun, W. Xiang, C. Shen, Z. Wang, X. Jia, J. Sun, C. J. Liu, *Nano Energy* **2020**, *76*, 104998.
[196] Z. Wang, Y. Liu, P. Tao, Q. Shen, N. Yi, F. Zhang, Q. Liu, C. Song, D. Zhang, W. Shang, T. Deng, *Small* **2014**, *10*, 3234.
[197] P. Tao, G. Ni, C. Song, W. Shang, J. Wu, J. Zhu, G. Chen, T. Deng, *Nat. Energy* **2018**, *3*, 1031.
[198] H. Liu, Z. Huang, K. Liu, X. Hu, J. Zhou, *Adv. Energy Mater.* **2019**, *9*, 1900310.
[199] V. D. Dao, N. H. Vu, S. Yun, *Nano Energy* **2020**, *68*, 104324.
[200] K. Vynck, M. Burresi, F. Riboli, D. S. Wiersma, *Nat. Mater.* **2012**, *11*, 1017.
[201] Y. F. Huang, S. Chattopadhyay, Y. J. Jen, C. Y. Peng, T. A. Liu, Y. K. Hsu, C. L. Pan, H. C. Lo, C. H. Hsu, Y. H. Chang, C. S. Lee, K. H. Chen, L. C. Chen, *Nat. Nanotechnol.* **2007**, *2*, 770.
[202] M. Shang, N. Li, S. Zhang, T. Zhao, C. Zhang, C. Liu, H. Li, Z. Wang, *ACS Appl. Energy Mater.* **2018**, *1*, 56.
[203] L. Mascaretti, A. Schirato, R. Zbořil, Š. Kment, P. Schmuki, A. Alabastri, A. Naldoni, *Nano Energy* **2021**, *83*, 105828.
[204] E. H. Ang, Y. Z. Tan, J. W. Chew, *J. Mater. Chem. A* **2019**, *7*, 10206.
[205] A. Politano, G. Di Profio, E. Fontananova, V. Sanna, A. Cupolillo, E. Curcio, *Desalination* **2019**, *451*, 192.
[206] Y. Huang, Y. Morishita, K. Uetani, M. Nogi, H. Koga, *Nanoscale Adv.* **2020**, *2*, 2339.
[207] M. Zhu, Y. Li, F. Chen, X. Zhu, J. Dai, Y. Li, Z. Yang, X. Yan, J. Song, Y. Wang, E. Hitz, W. Luo, M. Lu, B. Yang, L. Hu, *Adv. Energy Mater.* **2018**, *8*, 1701028.
[208] C. Sheng, N. Yang, Y. Yan, X. Shen, C. Jin, Z. Wang, Q. Sun, *Appl. Therm. Eng.* **2020**, *167*, 114712.
[209] H. Ghasemi, G. Ni, A. M. Marconnet, J. Loomis, S. Yerci, N. Miljkovic, G. Chen, *Nat. Commun.* **2014**, *5*, 4449.
[210] W. Shang, T. Deng, *Nat. Energy* **2016**, *1*, 16133.
[211] G. Baffou, R. Quidant, *Chem. Soc. Rev.* **2014**, *43*, 3898.
[212] M. Ghoussoub, M. Xia, P. N. Duchesne, D. Segal, G. Ozin, *Energy Environ. Sci.* **2019**, *12*, 1122.
[213] D. Mateo, J. L. Cerrillo, S. Durini, J. Gascon, *Chem. Soc. Rev.* **2021**, *50*, 2173.
[214] L. Zhou, D. F. Swearer, H. Robatjazi, A. Alabastri, P. Christopher, E. A. Carter, P. Nordlander, N. J. Halas, *Science* **2019**, *364*, 279.
[215] X. Li, H. O. Everitt, J. Liu, *Nano Res.* **2020**, *13*, 1268.
[216] G. Baffou, I. Bordacchini, A. Baldi, R. Quidant, *Light: Sci. Appl.* **2020**, *9*, 108.
[217] D. A. Boyd, L. Greengard, M. Brongersma, M. Y. El-Naggar, D. G. Goodwin, *Nano Lett.* **2006**, *6*, 2592.
[218] L. Cao, D. N. Barsic, A. R. Guichard, M. L. Brongersma, *Nano Lett.* **2007**, *7*, 3523.
[219] I. L. Violi, J. Gargiulo, C. von Bilderling, E. Cortés, F. D. Stefani, *Nano Lett.* **2016**, *16*, 6529.
[220] R. Kamarudheen, G. Kumari, A. Baldi, *Nat. Commun.* **2020**, *11*, 3957.

[221] R. Kamarudheen, G. J. W. Aalbers, R. F. Hamans, L. P. J. Kamp, A. Baldi, *ACS Energy Lett.* **2020**, *5*, 2605.
[222] B. J. Roxworthy, A. M. Bhuiya, V. V. G. K. Inavalli, H. Chen, K. C. Toussaint, *Nano Lett.* **2014**, *14*, 4687.
[223] E. C. Garnett, W. Cai, J. J. Cha, F. Mahmood, S. T. Connor, M. G. Christoforo, Y. Cui, M. D. Mcgehee, M. L. Brongersma, *Nat. Mater.* **2012**, *11*, 241.
[224] M. Valenti, M. P. Jonsson, G. Biskos, A. Schmidt-Ott, W. A. Smith, *J. Mater. Chem. A* **2016**, *4*, 17891.
[225] A. Lenert, D. M. Bierman, Y. Nam, W. R. Chan, I. Celanović, M. Soljačić, E. N. Wang, *Nat. Nanotechnol.* **2014**, *9*, 126.
[226] J. C. Matsubu, V. N. Yang, P. Christopher, *J. Am. Chem. Soc.* **2015**, *137*, 3076.
[227] N. Zhang, M. Q. Yang, S. Liu, Y. Sun, Y. J. Xu, *Chem. Rev.* **2015**, *115*, 10307.
[228] S. Mukherjee, L. Zhou, A. M. Goodman, N. Large, C. Ayala-Orozco, Y. Zhang, P. Nordlander, N. J. Halas, *J. Am. Chem. Soc.* **2014**, *136*, 64.
[229] P. Christopher, H. Xin, S. Linic, *Nat. Chem.* **2011**, *3*, 467.
[230] L. Zhou, C. Zhang, M. J. McClain, A. Manjavacas, C. M. Krauter, S. Tian, F. Berg, H. O. Everitt, E. A. Carter, P. Nordlander, N. J. Halas, *Nano Lett.* **2016**, *16*, 1478.
[231] J. R. Adleman, D. A. Boyd, D. G. Goodwin, D. Psaltis, *Nano Lett.* **2009**, *9*, 4417.
[232] M. Kim, S. M. Ko, J. M. Nam, *Nanoscale* **2016**, *8*, 11707.
[233] D. F. Swearer, H. Zhao, L. Zhou, C. Zhang, H. Robatjazi, J. M. P. Martirez, C. M. Krauter, S. Yazdi, M. J. McClain, E. Ringe, E. A. Carter, P. Nordlander, N. J. Halas, *Proc. Natl. Acad. Sci. USA* **2016**, *113*, 8916.
[234] C. Zhang, H. Zhao, L. Zhou, A. E. Schlather, L. Dong, M. J. McClain, D. F. Swearer, P. Nordlander, N. J. Halas, *Nano Lett.* **2016**, *16*, 6677.
[235] D. F. Swearer, R. K. Leary, R. Newell, S. Yazdi, H. Robatjazi, Y. Zhang, D. Renard, P. Nordlander, P. A. Midgley, N. J. Halas, E. Ringe, *ACS Nano* **2017**, *11*, 10281.
[236] F. Wang, C. Li, H. Chen, R. Jiang, L. D. Sun, Q. Li, J. Wang, J. C. Yu, C. H. Yan, *J. Am. Chem. Soc.* **2013**, *135*, 5588.
[237] L. Wang, Y. Dong, T. Yan, Z. Hu, A. A. Jelle, D. M. Meira, P. N. Duchesne, J. Y. Y. Loh, C. Qiu, E. E. Storey, Y. Xu, W. Sun, M. Ghoussoub, N. P. Kherani, A. S. Helmy, G. A. Ozin, *Nat. Commun.* **2020**, *11*, 2432.
[238] J. Quiroz, E. C. M. Barbosa, T. P. Araujo, J. L. Fiorio, Y. C. Wang, Y. C. Zou, T. Mou, T. V. Alves, D. C. de Oliveira, B. Wang, S. J. Haigh, L. M. Rossi, P. H. C. Camargo, *Nano Lett.* **2018**, *18*, 7289.
[239] U. Aslam, S. Chavez, S. Linic, *Nat. Nanotechnol.* **2017**, *12*, 1000.
[240] F. Wang, Y. Huang, Z. Chai, M. Zeng, Q. Li, Y. Wang, D. Xu, *Chem. Sci.* **2016**, *7*, 6887.
[241] Q. L. Zhu, J. Li, Q. Xu, *J. Am. Chem. Soc.* **2013**, *135*, 10210.
[242] H.-C. Ma, C.-C. Zhao, G.-J. Chen, Y.-B. Dong, *Nat. Commun.* **2019**, *10*, 3368.
[243] H. Jia, A. Du, H. Zhang, J. Yang, R. Jiang, J. Wang, C. Y. Zhang, *J. Am. Chem. Soc.* **2019**, *141*, 5083.
[244] K. Li, N. J. Hogan, M. J. Kale, N. J. Halas, P. Nordlander, P. Christopher, *Nano Lett.* **2017**, *17*, 3710.
[245] E. T. Swartz, R. O. Pohl, *Rev. Mod. Phys.* **1989**, *61*, 605.
[246] Q. Zhang, X. Jin, Z. Xu, J. Zhang, U. F. Rendón, L. Razzari, M. Chaker, D. Ma, *J. Phys. Chem. Lett.* **2018**, *9*, 5317.
[247] C. Clavero, *Nat. Photonics* **2014**, *8*, 95.
[248] G. Tagliabue, J. S. DuChene, M. Abdellah, A. Habib, D. J. Gosztola, Y. Hattori, W.-H. Cheng, K. Zheng, S. E. Canton, R. Sundararaman, J. Sá, H. A. Atwater, *Nat. Mater.* **2020**, *19*, 1312.
[249] A. Naldoni, Z. A. Kudyshev, L. Mascaretti, S. P. Sarmah, S. Rej, J. P. Froning, O. Tomanec, J. E. Yoo, D. Wang, Š. Kment, T. Montini, P. Fornasiero, V. M. Shalaev, P. Schmuki, A. Boltasseva, R. Zbořil, *Nano Lett.* **2020**, *20*, 3663.
[250] M. Gao, C. K. Peh, L. Zhu, G. Yilmaz, G. W. Ho, *Adv. Energy Mater.* **2020**, *10*, 2000925.
[251] P. D. Dongare, Y. Zhao, D. Renard, J. Yang, O. Neumann, J. Metz, L. Yuan, A. Alabastri, P. Nordlander, N. J. Halas, *ACS Nano* **2021**, *15*, 8761.
[252] N.-P. Harder, P. Würfel, *Semicond. Sci. Technol.* **2003**, *18*, S151.
[253] Z. Zhou, E. Sakr, Y. Sun, P. Bermel, *Nanophotonics* **2016**, *5*, 1.
[254] H. Wang, J. Y. Chang, Y. Yang, L. Wang, *Int. J. Heat Mass Transfer* **2016**, *98*, 788.
[255] X. Luo, D. Tsai, M. Gu, M. Hong, *Chem. Soc. Rev.* **2019**, *48*, 2458.
[256] M. Shimizu, A. Kohiyama, H. Yugami, *J. Photonics Energy* **2015**, *5*, 053099.
[257] A. Kohiyama, M. Shimizu, H. Yugami, *Appl. Phys. Express* **2016**, *9*, 112302.
[258] S. Ogawa, M. Kimata, *Materials* **2018**, *11*, 458.
[259] Y. Li, D. Li, D. Zhou, C. Chi, S. Yang, B. Huang, *Sol. RRL* **2018**, *2*, 1800057.
[260] H. Wang, Q. Chen, L. Wen, S. Song, X. Hu, G. Xu, *Photonics Res.* **2015**, *3*, 329.
[261] D. N. Woolf, E. A. Kadlec, D. Bethke, A. D. Grine, J. J. Nogan, J. G. Cederberg, D. B. Burckel, T. S. Luk, E. A. Shaner, J. M. Hensley, *Optica* **2018**, *5*, 213.
[262] D. G. Baranov, Y. Xiao, I. A. Nechepurenko, A. Krasnok, A. Alù, M. A. Kats, *Nat. Mater.* **2019**, *18*, 920.
[263] X. Yu, J. Chan, C. Chen, *Nano Energy* **2021**, *88*, 106259.
[264] J. long Kou, Z. Jurado, Z. Chen, S. Fan, A. J. Minnich, *ACS Photonics* **2017**, *4*, 626.
[265] D. Li, X. Liu, W. Li, Z. Lin, B. Zhu, Z. Li, J. Li, B. Li, S. Fan, J. Xie, J. Zhu, *Nat. Nanotechnol.* **2021**, *16*, 153.
[266] S. Zeng, S. Pian, M. Su, Z. Wang, M. Wu, X. Liu, M. Chen, Y. Xiang, J. Wu, M. Zhang, Q. Cen, Y. Tang, X. Zhou, Z. Huang, R. Wang, A. Tunuhe, X. Sun, Z. Xia, M. Tian, M. Chen, X. Ma, L. Yang, J. Zhou, H. Zhou, Q. Yang, X. Li, Y. Ma, G. Tao, *Science* **2021**, *373*, 692.
[267] X. Yin, R. Yang, G. Tan, S. Fan, *Science* **2020**, *370*, 786.
[268] X. Wang, H. He, J. Gao, H. Hu, S. Tang, X. Li, X. Li, H. Cao, *J. Mater.* **2021**, *7*, 1103.
[269] M. G. Tsegay, H. G. Gebretinsae, J. Sackey, C. J. Arendse, Z. Y. Nuru, *Mater. Today: Proc.* **2019**, *36*, 571.
[270] C. Wang, W. Li, Z. Li, B. Fang, *Renewable Sustainable Energy Rev.* **2020**, *134*, 110277.
[271] F. Cao, K. McEnaney, G. Chen, Z. Ren, *Energy Environ. Sci.* **2014**, *7*, 1615.
[272] G. Albrecht, S. Kaiser, H. Giessen, M. Hentschel, *Nano Lett.* **2017**, *17*, 6402.
[273] Y. Li, C. Lin, Z. Wu, Z. Chen, C. Chi, F. Cao, D. Mei, H. Yan, C. Y. Tso, C. Y. H. Chao, B. Huang, *Adv. Mater.* **2021**, *33*, 14.
[274] A. Raza, A. S. Alketbi, R. Devarapalli, H. Li, T. Zhang, *Adv. Opt. Mater.* **2020**, *8*, 2000679.
[275] T. Inoue, M. De Zoysa, T. Asano, S. Noda, *Optica* **2015**, *2*, 27.
[276] K. Aydin, V. E. Ferry, R. M. Briggs, H. A. Atwater, *Nat. Commun.* **2011**, *2*, 517.
[277] D. Shin, G. Kang, P. Gupta, S. Behera, H. Lee, A. M. Urbas, W. Park, K. Kim, *Adv. Opt. Mater.* **2018**, *6*, 1800317.
[278] H. Cai, Y. Sun, X. Wang, S. Zhan, *Opt. Express* **2020**, *28*, 15347.
[279] M. Zhang, J. Fang, F. Zhang, J. Chen, H. Yu, *Opt. Commun.* **2017**, *405*, 216.
[280] S. Behera, J. Joseph, *J. Appl. Phys.* **2017**, *122*, 193104.
[281] A. Nagarajan, K. Vivek, M. Shah, V. G. Achanta, G. Gerini, *Adv. Opt. Mater.* **2018**, *6*, 1800253.
[282] L. P. Wang, Z. M. Zhang, *Appl. Phys. Lett.* **2012**, *100*, 2010.
[283] H. Wang, L. Wang, *Opt. Express* **2013**, *21*, A1078.
[284] D. Woolf, J. Hensley, J. G. Cederberg, D. T. Bethke, A. D. Grine, E. A. Shaner, *Appl. Phys. Lett.* **2014**, *105*, 081110.
[285] E. Rephaeli, S. Fan, *Opt. Express* **2009**, *17*, 15145.

[286] V. Rinnerbauer, A. Lenert, D. M. Bierman, Y. X. Yeng, W. R. Chan, R. D. Geil, J. J. Senkevich, J. D. Joannopoulos, E. N. Wang, M. Soljačič, I. Celanovic, *Adv. Energy Mater.* **2014**, *4*, 1400334.
[287] K. Cui, P. Lemaire, H. Zhao, T. Savas, G. Parsons, A. J. Hart, *Adv. Energy Mater.* **2018**, *8*, 1801471.
[288] T. Inoue, T. Koyama, D. D. Kang, K. Ikeda, T. Asano, S. Noda, *Nano Lett.* **2019**, *19*, 3948.
[289] A. Fiorino, L. Zhu, D. Thompson, R. Mittapally, P. Reddy, E. Meyhofer, *Nat. Nanotechnol.* **2018**, *13*, 806.
[290] S. Jin, M. Lim, S. S. Lee, B. J. Lee, *Opt. Express* **2016**, *24*, A635.
[291] O. Ilic, M. Jablan, J. D. Joannopoulos, I. Celanovic, M. Soljačić, *Opt. Express* **2012**, *20*, A366.
[292] Z. Omair, G. Scranton, L. M. Pazos-Outón, T. P. Xiao, M. A. Steiner, V. Ganapati, P. F. Peterson, J. Holzrichter, H. Atwater, E. Yablonovitch, *Proc. Natl. Acad. Sci. USA* **2019**, *116*, 15356.
[293] Z. Wang, Z. Tong, Q. Ye, H. Hu, X. Nie, C. Yan, W. Shang, C. Song, J. Wu, J. Wang, H. Bao, P. Tao, T. Deng, *Nat. Commun.* **2017**, *8*, 1478.
[294] T. Burger, C. Sempere, B. Roy-Layinde, A. Lenert, *Joule* **2020**, *4*, 1660.
[295] X. Wang, G. Ou, N. Wang, H. Wu, *ACS Appl. Mater. Interfaces* **2016**, *8*, 9194.
[296] N. Horiuchi, *Nat. Photonics* **2020**, *14*, 66.
[297] J. Song, L. Lu, B. Li, B. Zhang, R. Hu, X. Zhou, Q. Cheng, *Int. J. Heat Mass Transfer* **2020**, *150*, 119346.
[298] N. H. Thomas, M. C. Sherrott, J. Broulliet, H. A. Atwater, A. J. Minnich, *Nano Lett.* **2019**, *19*, 3898.
[299] Y. Li, C. Xiong, H. Huang, X. Peng, D. Mei, M. Li, G. Liu, M. Wu, T. Zhao, B. Huang, *Adv. Mater.* **2021**, *33*, 2103054.
[300] M.-N. Su, C. J. Ciccarino, S. Kumar, P. D. Dongare, S. A. H. Jebeli, D. Renard, Y. Zhang, B. Ostovar, W.-S. Chang, P. Nordlander, N. J. Halas, R. Sundararaman, P. Narang, S. Link, *Nano Letters* **2019**, *19*, 3091.

Bei Yang is a Postdoc in Qing Dai's group in the National Center of Nanoscience and Technology, China. She received her B.Sc. in Thermal Engineering from the Wuhan University of Technology in 2013 and Ph.D. in Electrical Engineering from the Institute of Electrical Engineering, Chinese Academy of Sciences in 2020. Her main research interests lie in energy materials, solar thermal utilization, highly efficient photothermal conversion, thermophotonics, and nanophotonics.

Zhifeng Wang is a Professor of the Institute of Electrical Engineering, Chinese Academy of Sciences, China. He received his M.Sc. in Materials from the Wuhan University of Technology in 1990 and Ph.D. in Thermal Engineering from the Tsinghua University in 1993. His main interests are solar thermal power generation, solar thermal utilization, highly efficient energy conversion and utilization, and large-scale seasonal thermal energy storage.

Qing Dai is a Professor of the National Center of Nanoscience and Technology, China. He received his M.Eng. in Electronic and Electrical Engineering from the Imperial College, London, in 2007 and Ph.D. in Nanophotonics from the Department of Engineering, University of Cambridge in 2011. His main research interests are low-dimensional materials, optoelectronics, nanophotonics, and thermophotonics.